nature microbiology

Article

https://doi.org/10.1038/s41564-024-01795-7

Single-cell detection of copy number changes reveals dynamic mechanisms of adaptation to antifungals in *Candida albicans*

Received: 16 December 2023

Accepted: 24 July 2024

Published online: 03 September 2024

Check for updates

Xin Zhou[1], Audrey Hilk[1], Norma V. Solis[2], Nancy Scott[1], Annette Beach[1], Natthapon Soisangwan[1], Clara L. Billings[3], Laura S. Burrack[3], Scott G. Filler[2,4] & Anna Selmecki[1]

Genomic copy number changes are associated with antifungal drug resistance and virulence across diverse fungal pathogens, but the rate and dynamics of these genomic changes in the presence of antifungal drugs are unknown. Here we optimized a dual-fluorescent reporter system in the diploid pathogen *Candida albicans* to quantify haplotype-specific copy number variation (CNV) and loss of heterozygosity (LOH) at the single-cell level with flow cytometry. We followed the frequency and dynamics of CNV and LOH at two distinct genomic locations in the presence and absence of antifungal drugs in vitro and in a murine model of candidiasis. Copy number changes were rapid and dynamic during adaptation to fluconazole and frequently involved competing subpopulations with distinct genotypes. This study provides quantitative evidence for the rapid speed at which diverse genotypes arise and undergo dynamic population-level fluctuations during adaptation to antifungal drugs in vitro and in vivo.

Candida albicans, the most prevalent human fungal pathogen, causes deadly invasive infections in immunocompromised individuals, with mortality rates of 20–60% despite antifungal treatment[1–5]. Fluconazole (FLC) is a triazole antifungal that is commonly used to treat *C. albicans* infections due to its water solubility, linear pharmacokinetics and excellent distribution into diverse tissues[6]. FLC is fungistatic rather than fungicidal and reaches a range of physiological concentrations that promote adaptation to the drug[6–8]. FLC can select for large-scale genomic changes including copy number variation (CNV) involving whole and segmental chromosomes, loss of heterozygosity (LOH) and polyploidy in diverse *Candida* species[8–16]. These large-scale genomic changes are common in *C. albicans* clinical isolates and cells recovered from infected mice[8,17–21].

Antifungal concentration impacts the acquisition of resistance and tolerance phenotypes. Antifungal resistance is the ability to grow well at drug concentrations above the minimum inhibitory concentration (MIC) of drug susceptible isolates at 24 h. Antifungal tolerance is a distinct phenotype from resistance, in which susceptible isolates grow slowly above the MIC at 48 h in a drug concentration-independent manner[22–24]. Experimental evolution with *C. albicans* identified that on average, drug resistance emerges at concentrations of FLC near the MIC, whereas drug tolerance emerges at concentrations above the MIC (supra-MIC)[23,25]. However, the impact of drug concentration on the frequency of drug resistance and tolerance-associated copy number changes is not known.

A common mechanism of acquired drug resistance across human fungal pathogens is via the acquisition of aneuploidy, amplification

[1]Department of Microbiology and Immunology, University of Minnesota, Minneapolis, MN, USA. [2]Division of Infectious Diseases, Lundquist Institute for Biomedical Innovation at Harbor UCLA Medical Center, Torrance, CA, USA. [3]Gustavus Adolphus College, Department of Biology, Saint Peter, MN, USA. [4]David Geffen School of Medicine at UCLA, Los Angeles, CA, USA. e-mail: selmecki@umn.edu

of an entire chromosome or chromosome segment[7,9,12,20,23,25–30]. In *C. albicans*, Chr5 is the most commonly amplified chromosome in azole-resistant clinical isolates[8,10,23,26–30]. Chr5 contains *ERG11* and *TAC1*, encoding the azole target and a transcriptional regulator of drug efflux pumps, and amplification of these two genes via aneuploidy or an isochromosome of the left arm of Chr5 (i(5L)) causes multi-azole resistance[8,9,30]. In addition, aneuploidy of other chromosomes including Chr3, Chr6 and ChrR is common during in vitro adaptation to azoles or other drugs[10,23,25,27,30–33]. Similar to Chr5, Chr3 contains key genes involved in drug resistance including two drug efflux pumps encoded by *CDR1* and *CDR2*, and a multidrug resistance regulator encoded by *MRR1* that activates a third drug efflux pump encoded by *MDR1* on Chr6 (refs. 27,28,34–36). LOH of *MRR1* or *TAC1* alleles with gain-of-function mutations can cause constitutive upregulation of drug efflux pumps and drug resistance[34,37]. Both amplification and LOH of beneficial alleles on Chr3 and Chr5 can cause resistance, yet we lack a quantitative understanding of the rate and dynamics of DNA copy number changes that arise in fungal cells during adaptation to antifungal drugs.

Quantifying the emergence and spread of DNA copy number changes within a population of cells is challenging because these events can vary in both frequency and amplitude[10,38]. Recently, fluorescent reporter systems have been used to estimate DNA copy number changes at the single-cell level with flow cytometry, including CNVs in haploid *Saccharomyces cerevisiae*[39] and LOH in diploid *C. albicans*[40]. These reporters have identified genomic features that alter the frequency of CNV or LOH events, including recessive lethal alleles in *C. albicans*[40–46].

We optimized a dual-fluorescent reporter system to simultaneously detect CNV and LOH events at the single-cell level in *C. albicans*. We engineered heterozygous BFP/GFP loci at intergenic regions on Chr3 and Chr5 that we previously found to undergo amplification during adaptation to antifungal drugs[10,11]. We quantified the frequency and dynamics of fluorescent copy number changes during adaptation to different concentrations of FLC, both in vitro and in a mouse model of disseminated candidiasis. Genotypes corresponding to fluorescence changes were confirmed using extensive whole-genome sequencing (WGS). In vitro, we detected copy number changes as early as ~10 generations after drug exposure and multiple distinct lineages arose simultaneously within most populations, resulting in dynamic clonal interference. In the murine model, Chr3 and Chr5 copy number changes only occurred in isolates recovered from mice treated with FLC, including changes in whole-genome ploidy levels (polyploidization). Cells with concurrent aneuploidy of Chr3 and Chr6 arose both in vitro and in vivo, and this combination had a synergistic effect on multi-azole tolerance. This is presumably the first comprehensive analysis of the frequency, dynamics and fitness effects of copy number changes that occur during antifungal drug treatment both in vitro and in vivo at the single-cell level in any fungal species.

Results

Fluconazole selects for copy number changes on Chr3 and Chr5

We constructed dual-fluorescent BFP/GFP reporter strains of Chr3 and Chr5 to quantify the frequency and dynamics of haplotype-specific CNV and LOH events at the single-cell level with flow cytometry (Supplementary Tables 1 and 2). These strains have a 1:1 ratio of BFP:GFP on either Chr3 or Chr5. BFP/GFP changes correlating with copy number gain (CNV BFP or CNV GFP) and loss (GFP-only or BFP-only) were rigorously verified using flow cytometry. The specific haplotype (A or B) that carried the BFP or GFP allele in each strain was determined using WGS (Supplementary Note 1 and Extended Data Fig. 1).

Next, we determined the effect of FLC concentration on the frequency and dynamics of BFP/GFP changes. Twelve independent populations for each reporter strain were passaged at four different FLC concentrations (0, 1, 4 and 8 μg ml^{-1} FLC) for 10 passages (~100 generations, P1–P10), followed by another 5 passages in rich medium alone (~50 generations, P11–P15) (Supplementary Note 2 and Extended Data Fig. 2). The BFP/GFP reporter strains had an initial MIC of 0.5 μg ml^{-1} FLC, therefore 1 μg ml^{-1} FLC represented a near-MIC concentration, and 4 and 8 μg ml^{-1} FLC represented supra-MIC concentrations[23,25]. Flow cytometry analysis was performed at P0, P1, P5, P10, P12 and P15 to quantify the proportion of all fluorescent subpopulations over time. BFP/GFP changes predominantly occurred during adaptation to FLC and rarely in the absence of FLC (Fig. 1a,b). Approximately 75% (54/72) of the FLC-evolved populations had multiple distinct subpopulations with BFP/GFP changes that were co-evolving. Subpopulations with BFP/GFP changes typically increased in the presence of FLC over time (P1–P10) but decreased after removal of the drug (P10–P15) (Fig. 1c,d).

Drug concentration had different effects on Chr3 and Chr5 copy number dynamics. In 1 μg ml^{-1} FLC, almost all (10/12) Chr3 populations had a majority of cells with fluorescence changes at P10, compared with only a few (2/12) Chr5 populations at the same timepoint (Fig. 1a,b). In addition, there was a bias for the Chr3 GFP haplotype at all drug concentrations, exhibited as LOH at 1 μg ml^{-1} FLC and as CNV at 4 and 8 μg ml^{-1} FLC (Fig. 1a,c). These results highlight the specificity of copy number changes selected on the basis of chromosome, haplotype and drug concentration.

Population dynamics during adaptation to fluconazole

To quantify the dynamics of BFP/GFP copy number changes in FLC-evolved populations, we estimated several key parameters of asexual population dynamics including the time it takes for mutant lineages to appear within the population at detectable levels (T_{up}) and the estimated relative fitness of those mutant lineages (S_{up}) which is based on the rate at which these cells increase in the population per generation (Methods)[39,47]. To obtain higher resolution estimates of T_{up} and S_{up}, we increased the population sampling to every passage for ten lineages representing both Chr3 and Chr5 in all drug concentrations (Supplementary Table 3). BFP/GFP changes were detected as early as P1 (T_{up}) and had an estimated relative fitness advantage ranging from 1.060 to 1.727 (Supplementary Table 3 and Fig. 2a). The most rapid subpopulation expansion occurred in three Chr3-tagged lineages evolved in 1 or 4 μg ml^{-1} FLC (named by the tagged chromosome, FLC concentration and lineage number: Chr3_FLC1_L4, Chr3_FLC1_L9 and Chr3_FLC4_L8). In these three lineages, the GFP subpopulations (GFP only or CNV GFP) reached the maximum frequency (T_{peak}) after just two passages and had dramatically increased S_{up} ($1 + S_{up} = 1.591$, 1.672 and 1.727, respectively; Supplementary Table 3).

Upon removal of FLC (P11–P15), the frequency of CNVs decreased for almost all populations, while LOH increased or stayed the same (Figs. 1a,b and 2a), indicating that the CNVs might be unstable and/or incur a fitness cost. Therefore, we estimated the rate at which CNV subpopulations decreased in the population per generation (S_{down}) for eight FLC-evolved lineages ($1 + S_{down}$ ranged from 0.882 to 0.957; Extended Data Fig. 3 and Supplementary Table 3). As these CNVs disappeared from the population, BFP-only or GFP-only cells resulting from LOH events appeared and rapidly increased in frequency with $1 + S_{up}$ values ranging from 1.045 to 1.113 (Supplementary Table 3). Intriguingly, we observed a correlation between the CNV genotypes that dominated in P10 (for example, CNV GFP) and the LOH genotypes that subsequently replaced them (for example, GFP-only cells). Therefore, it is likely that some of the cells with CNV are undergoing non-disjunction events that result in loss of an aneuploid chromosome and a return to euploid copy number that is either heterozygous or homozygous for the amplified haplotype.

Rapid population sweeps are driven by increased fitness

To quantify relative fitness, we performed head-to-head competition experiments with select subpopulations relative to the wild-type

https://doi.org/10.1038/s41564-024-01795-7

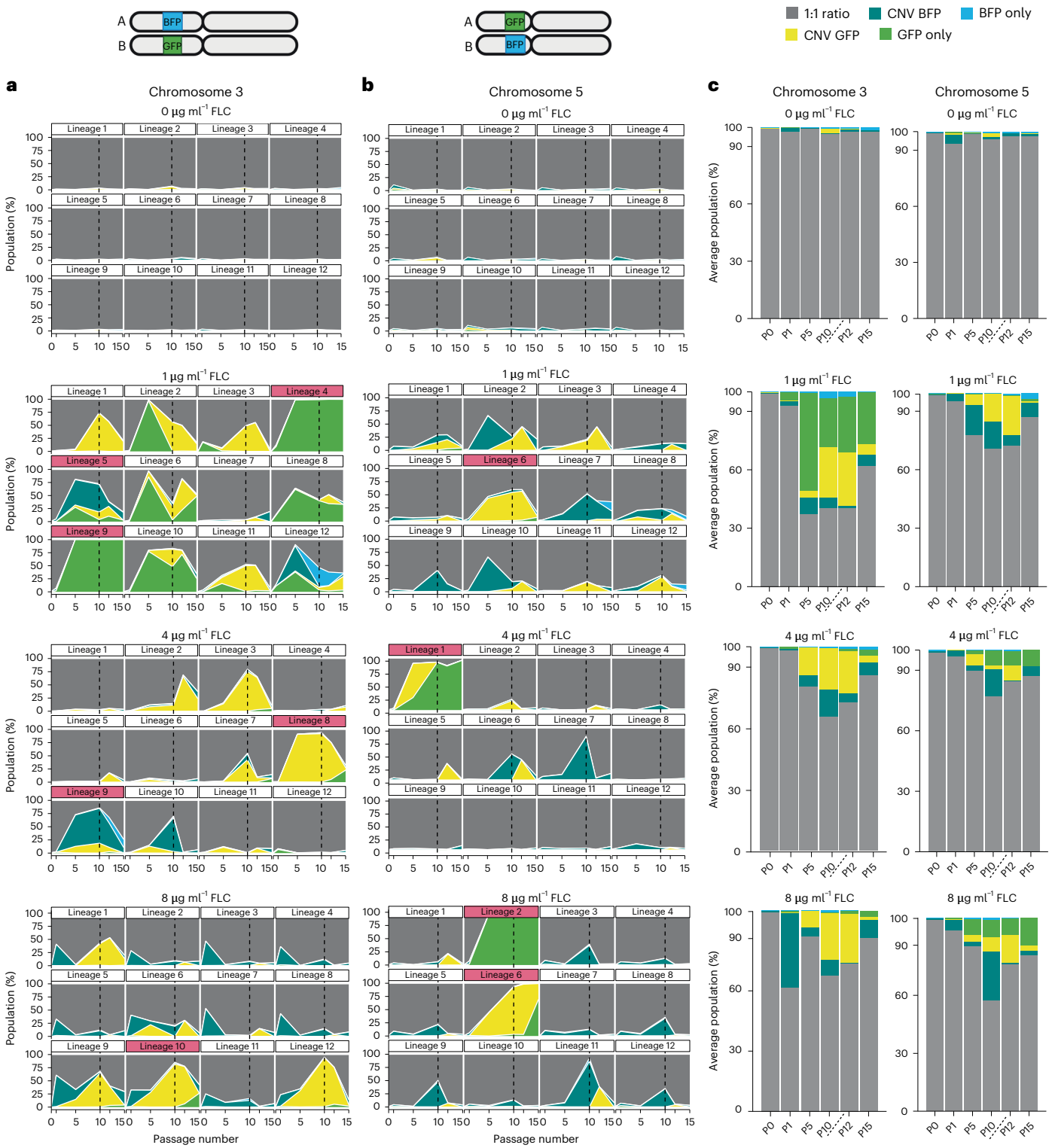

Fig. 1 | Fluconazole exposure selects for rapid and dynamic fluorescence changes on Chr3 and Chr5. Flow cytometry analysis of (**a**) Chr3 BFP/GFP and (**b**) Chr5 BFP/GFP lineages evolved in the absence or presence of FLC for 15 passages. Each graph represents the 12 independent lineages exposed to 0, 1, 4 or 8 μg ml^{-1} FLC. Flow cytometry data were collected at passages 0, 1, 5, 10, 12 and 15 (P0–P15). At P10 (dashed lines), no FLC was added to experiments to monitor stability of the fluorescent lineages in the absence of drug. The graph colours represent the fraction (%) of five different types of fluorescent cells within each population. Pink boxes indicate lineages selected for subsequent analysis (Fig. 2a). **c**, Average combined distributions from all 12 lineages at each drug concentration for the Chr3 (left) and the Chr5 (right) fluorescently tagged strains. Dashed lines indicate the time when no FLC was added to the experiments.

progenitor. We selected three FLC-evolved lineages where GFP-only cells took over the entire population by P10, exhibited high estimated relative fitness (S_{up}) and were stable after removal of the drug (Chr3_FLC1_L4, Chr3_FLC1_L9 and Chr5_FLC8_L2; Figs. 1a and 2a, and Supplementary Table 3). Clonal interference was evident in Chr5_FLC8_L2, where initially a CNV-GFP subpopulation appeared, but was replaced by the GFP-only subpopulation. This may explain the delay in time to fixation of the Chr5 GFP-only subpopulation (Fig. 2a). All three GFP-only

https://doi.org/10.1038/s41564-024-01795-7

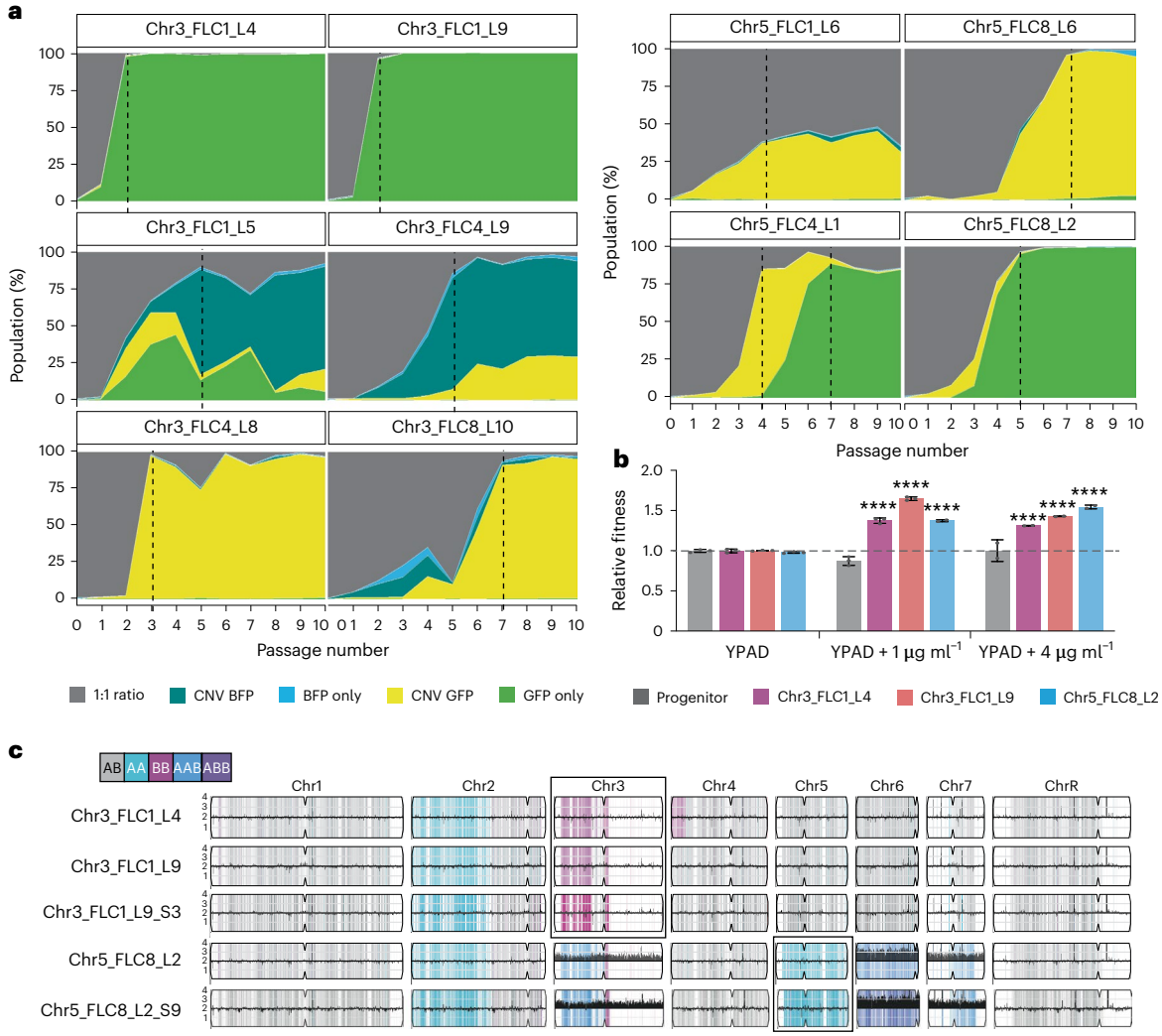

Fig. 2 | Rapid population sweeps are driven by increased fitness. a, Increased population sampling for select lineages of Chr3 (left) and Chr5 (right) during FLC adaptation (daily, P0–P10). Stacked population fractions presented as in Fig. 1. Dashed lines indicate T_{peak}. **b**, Relative fitness determined using a head-to-head competition over 48 h. Each GFP-only subpopulation at P10 was competed with the wild-type (non-fluorescent) control. Values are mean ± s.e.m. calculated from 3 biological replicates. Data were assessed for normality with a Shapiro–Wilk test, and significant differences between the progenitor and GFP lineages across different environments were calculated using two-way ANOVA with Dunnett's multiple comparisons test (two-sided); ****$P < 0.0001$; the exact P values were <0.0001 for all indicated comparisons. The dashed line indicates wild-type fitness. **c**, WGS data for the whole population of three GFP-only lineages (L4, L9 and L2) and single cells isolated from two of the same lineages at P10 (L9_S3 and L2_S9). WGS data are plotted as the $\log_2$ ratio and converted to chromosome copy number (y axis, 1–4 copies) as a function of chromosome position (x axis, Chr1–ChrR)[77]. The baseline ploidy was determined by propidium iodide (PI)-DNA staining (Supplementary Table 1). Haplotypes relative to the reference genome SC5314 are indicated: grey is heterozygous AB, magenta is homozygous B, cyan is homozygous A, purple is trisomy ABB and blue is trisomy AAB. Boxes highlight the BFP/GFP-tagged chromosome in each strain.

subpopulations had significantly increased competitive fitness relative to the progenitor in the presence of FLC ($P < 0.0001$; Fig. 2b). The competitive fitness of these three lineages was consistent with the estimated relative fitness (S_{up}) inferred from the population dynamics, especially for Chr3_FLC1_L9 ($1 + S_{up}$ of 1.672 and competitive fitness of 1.636; Supplementary Table 3 and Fig. 2b). These results support the idea that in general, the subpopulation expansions observed correlate with increased fitness.

We then used WGS to genotype the whole population of the three GFP-only lineages at P10 and a single colony from Chr3_FLC1_L9 and Chr5_FLC8_L2. These GFP-only lineages underwent LOH of the GFP-tagged chromosome and reduplicated the remaining homologue resulting in the following genotypes: Chr3BB and Chr5AA at both the population and single-cell level (Fig. 2c). The Chr3 GFP-only lineages were disomic for all other chromosomes, whereas the Chr5 GFP-only lineage acquired three additional chromosome aneuploidies with extra copies of Chr3, Chr6 and Chr7 (Fig. 2c). Variant calling revealed 11 de novo missense mutations across the three lineages, but none were recurrent or in known drug-related genes (Supplementary Table 4). These results suggest that the increased fitness for the Chr3 GFP-only lineages is caused by homozygosis of Chr3BB, while increased fitness for the Chr5 lineage might involve multiple genomic changes.

Chr3BB LOH correlates with increased fitness in drug

To determine whether LOH alone was sufficient to increase fitness in FLC even without previous drug exposure, we used fluorescence-activated cell sorting (FACS) to isolate GFP-only or BFP-only single cells from four independent 36 h cultures of the BFP/GFP progenitor strains (Fig. 3a). These cells were never exposed to FLC. Interestingly, we found that Chr3 GFP-only cells were significantly less frequent than Chr3 BFP-only cells after overnight growth in rich media (0.7×10^{-4} versus 4×10^{-4} events per total singlets; Fig. 3b, $P < 0.0001$, two-way analysis of variance

https://doi.org/10.1038/s41564-024-01795-7

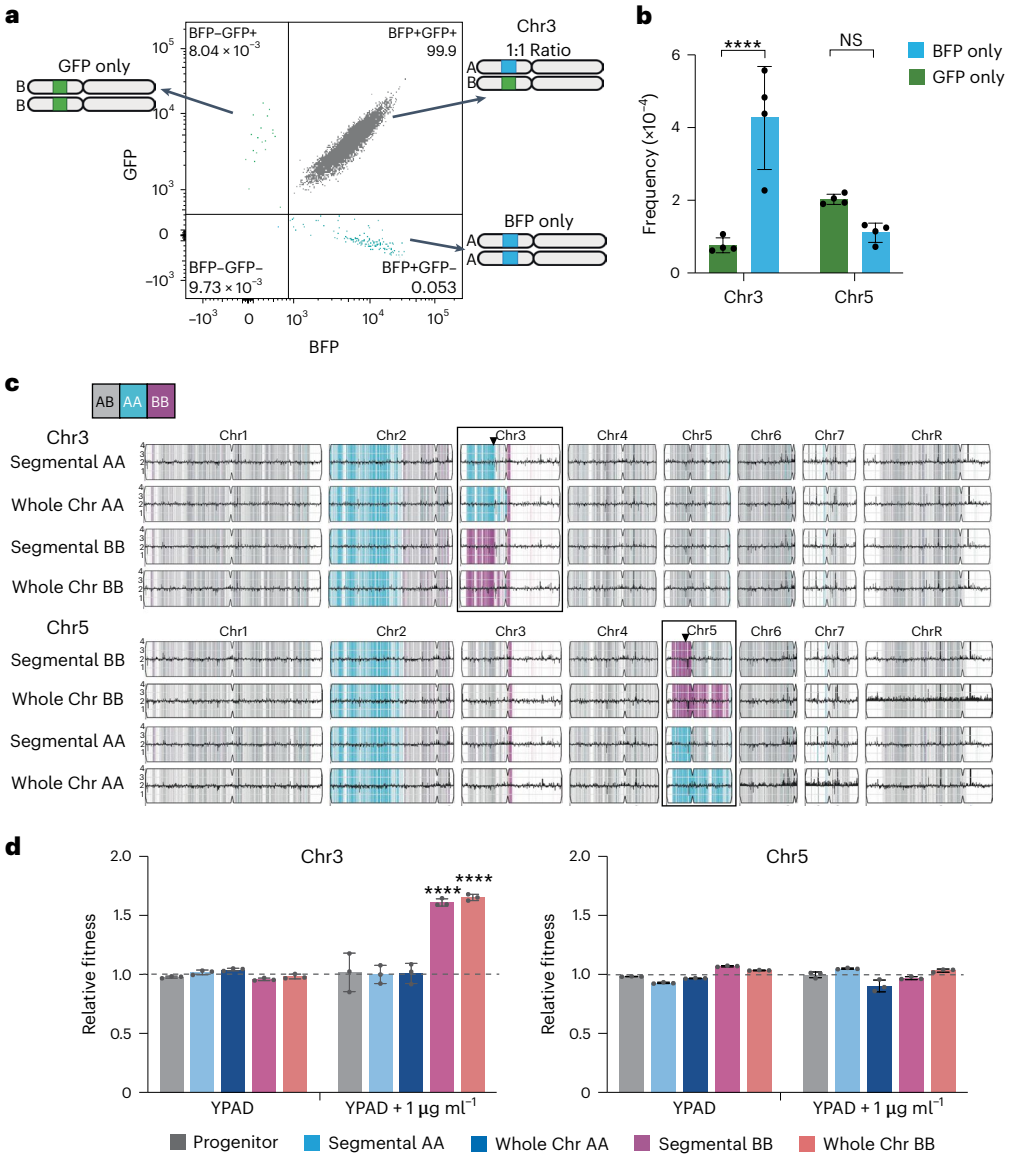

Fig. 3 | Single-cell sorting identifies different frequency and fitness consequences of Chr3 LOH. a, FACS of the BFP/GFP progenitor strains for BFP-only and GFP-only cells (Chr3 as representative) (Methods). **b**, Frequency of GFP-only and BFP-only cells detected by FACS of at least 10^5 cells from the Chr3 and Chr5 BFP/GFP progenitor populations after just 36 h growth in rich medium (YPAD). Values are mean ± s.e.m. calculated from 4 biological replicates. Data were assessed for normality using a Shapiro–Wilk test, and significant differences between the BFP only and GFP only were calculated using two-way ANOVA with Šídák's multiple comparisons test (two-sided); ****$P < 0.0001$; NS, $P > 0.05$; the exact P value for **** was <0.0001. **c**, Representative WGS data for BFP-only or GFP-only cells isolated from single-cell sorting, plotted as in Fig. 2 (all single-cell WGS data presented in Extended Data Fig. 4a,b). Whole-chromosome and segmental chromosome LOH of each haplotype (AA and BB) are indicated for single cells isolated from the Chr3- and Chr5-tagged strains by FACS. No other copy number changes were detected in these single cells. Haplotypes are indicated by the colour: grey is heterozygous AB, magenta is homozygous B and cyan is homozygous A. Boxes highlight the tagged chromosome. **d**, Relative fitness, determined by head-to-head competition, for single cells with LOH from **c** and the progenitor compared to the wild-type control for Chr3 (left) and Chr5 (right) LOH single cells. Values are mean ± s.e.m. calculated from 3 biological replicates. Data were assessed for normality by a Shapiro–Wilk test and significant differences between the progenitor and LOH single cells across different environments were calculated using two-way ANOVA with Dunnett's multiple comparisons test (two-sided). Chr3BB versus the progenitor: ****$P < 0.0001$; the exact P values were <0.0001 for all indicated comparisons. The dashed line indicates wild-type fitness.

(ANOVA)). There was no significant difference between the frequency of Chr5 GFP-only and BFP-only cells (2×10^{-4} and 1×10^{-4} events per total singlets; Fig. 3b). We genotyped 26 FACS-isolated single cells and found that all 26 were diploid and had undergone LOH of the tagged chromosome, followed by duplication of the remaining homologue, resulting in AA or BB genotypes (Extended Data Fig. 4 and Supplementary Table 1). LOH events included whole and segmental chromosome LOH, and gene conversion events involved just LOH of the fluorescent reporter (Extended Data Fig. 4). Only 1/26 single cells had copy number changes on any other chromosome.

We then selected representative LOH single cells for fitness analysis (Fig. 3c). In the absence of FLC, there was no fitness difference between single cells with Chr3AA or Chr3BB haplotypes (whole Chr and segmental LOH), indicating that the difference in LOH frequency observed by FACS is not due to fitness. In the presence of 1 μg ml^{-1} FLC, single cells with the Chr3BB haplotype had significantly increased fitness compared with the Chr3AA haplotype and the progenitor (Fig. 3d). There were no fitness differences between Chr5 haplotypes (Fig. 3d). In summary, Chr3 LOH resulting in haplotype Chr3AA (BFP-only) occurs at a significantly higher frequency than haplotype Chr3BB (GFP-only)

https://doi.org/10.1038/s41564-024-01795-7

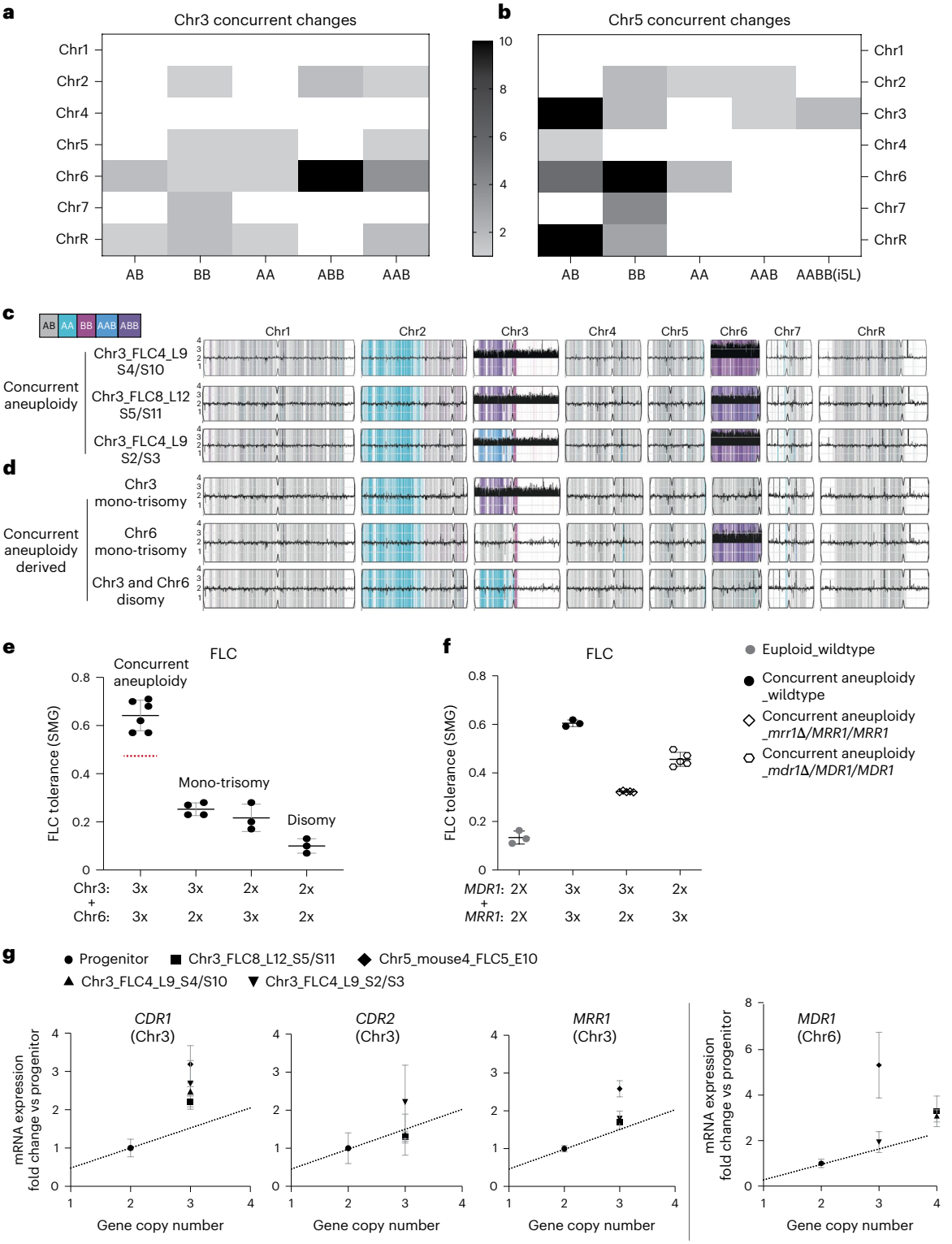

in rich media, but only Chr3BB provides a significant fitness benefit in the presence of FLC, which explains the rapid increase of this haplotype in many of the original 1 μg ml^{-1} FLC populations (Fig. 1a).

Chr3 and Chr6 act synergistically to confer azole tolerance

To identify genotypes responsible for increased fitness during adaptation to FLC in vitro, we isolated 53 single colonies from 16 FLC-evolved lineages with a majority of cells carrying BFP and/or GFP fluorescence changes. For each single colony, we quantified BFP/GFP fluorescence and performed WGS and ploidy analysis (Extended Data Fig. 5 and Supplementary Table 1). Copy number changes estimated from fluorescence phenotypes were highly consistent with WGS (Extended Data Fig. 6): all 18 BFP-only and GFP-only colonies had undergone LOH, including both segmental and whole Chr LOH (Extended Data Fig. 6a,b). A clear bias towards Chr3 haplotype B was again observed among Chr3 LOH strains (Fig. 2 and Extended Data Fig. 7a). Similarly, most of the 19 colonies with CNV acquired whole-chromosome trisomy resulting in genotypes Chr3AAB, Chr3ABB and Chr5AAB (Extended Data Figs. 6a,b and 7). Surprisingly, haplotype Chr5ABB was not confirmed via WGS, which was probably caused by the instability or

Fig. 4 | Synergistic effect of Chr3 and Chr6 aneuploidy on multi-azole tolerance. Number of chromosome copy number changes identified by WGS of the diploid FLC-evolved colonies ($n = 48$) from all three drug concentrations (Supplementary Table 1 and Extended Data Fig. 7). **a**, Chr3 BFP/GFP and **b**, Chr5 BFP/GFP. Heat map indicating the number of colonies with each pairwise combination. The *x* axis represents the Chr3 or Chr5 genotype and the *y* axis represents the other 7 untagged chromosomes. Genotypes include AB, BB, AA, ABB and AAB. Chr5 has an extra genotype of AABB (for i(5L)), but not ABB. **c**, WGS data for representative colonies from two independent FLC-evolved lineages with Chr3 trisomy (ABB or AAB) and Chr6 trisomy (ABB) or tetrasomy (ABBB), plotted as in Fig. 2. **d**, WGS data of three representative strains derived from strains in **c** that lost one or both aneuploid chromosomes (Supplementary Table 1), plotted as in Fig. 2. **c**,**d**, Haplotypes indicated by the colour grey designate heterozygous AB, magenta for homozygous B, cyan for homozygous A, purple for ABB and blue for AAB. **e**, FLC tolerance quantified as SMG for strains with Chr3 and Chr6 concurrent aneuploidy ($n = 6$ strains), Chr3 or Chr6 trisomy (mono-trisomy) ($n = 4$ and 3 strains, respectively), and no aneuploidy (disomy) ($n = 3$ strains). Red dashed line indicates the additive SMG value of Chr3 and Chr6 mono-trisomy strains. **f**, FLC tolerance (SMG) of the concurrent aneuploid strain with one copy of *MRR1* or one copy of *MDR1* deleted ($n = 5$ strains), compared to the concurrent aneuploid strain with the euploid progenitor as the control. Each dot represents independent transformants. **e**,**f**, Each dot represents the average of 3 technical replicates for each strain. The line and error bars indicate the median ± s.d. across all strains with the same genotype. **g**, mRNA expression fold change (*y* axis) of *CDR1*, *CDR2*, *MRR1* and *MDR1* in strains with Chr3 and Chr6 concurrent aneuploidy relative to the progenitor with *TEF1* on Chr2 as the control. Fold change is correlated with the gene copy number (*x* axis) and dotted lines indicate the expression level which increases proportionally with gene copy number. Dots and error bars indicate the average ± s.d. across 3 biological replicates.

fitness cost of this genotype (Supplementary Note 3 and Extended Data Fig. 7c). In addition to whole-chromosome aneuploidy, segmental amplification of Chr5L in an isochromosome (i(5L))[8,9] and whole-genome duplication events resulting in polyploid cells (ranging from triploid to tetraploid) were detected by dramatic increases in BFP/GFP fluorescence and confirmed with WGS and other techniques (Extended Data Fig. 6c,e). The consistency between fluorescence phenotypes and WGS data allows us to draw a direct connection between fluorescence changes and DNA copy number changes detected within FLC-evolved lineages.

Next, we determined the frequency of all other genomic changes that occurred concurrently with Chr3 and Chr5 changes in the 48 diploid colonies above (26 Chr3-tagged and 22 Chr5-tagged; Supplementary Table 1). Chr6 copy number changes, predominantly aneuploidy, were the most frequent of all untagged chromosomes (33/48 colonies; Fig. 4a,b and Extended Data Fig. 7). Concurrent aneuploidy of Chr3 and Chr6 (18/26 colonies) were frequently identified and most (15/18) had a bias for the B haplotype resulting in Chr6ABB trisomy or Chr6ABBB tetrasomy (Fig. 4c). Chr5 copy number changes also frequently had concurrent aneuploidy of Chr3 (12/22) and/or Chr6 (10/22) (Fig. 4b and Extended Data Fig. 7b,c).

We detected concurrent aneuploidy of Chr3 and Chr6 predominantly at supra-MIC concentrations of FLC (4 and 8 μg ml^{-1}). Previously, we found that high concentrations of FLC selects for evolved lineages with increased FLC tolerance, not resistance[23]. Therefore, we determined the concentration of drug that reduces growth by 50% (MIC_{50}) at 24 h (resistance) and supra-MIC growth (SMG) at 48 h (tolerance) in three different azole drugs for six strains that acquired concurrent aneuploidy of Chr3 and Chr6. All six aneuploid strains had high tolerance to all azoles tested, but only a 2-fold increase in FLC MIC (Fig. 4e and Extended Data Fig. 8a). To determine whether this multi-azole tolerance required both Chr3 and Chr6 aneuploidy, we isolated cells that had lost one or both aneuploidies from the concurrent aneuploid strains after ~60–80 generations in the absence of drug (Fig. 4d). Loss of the extra copy of either Chr3 or Chr6 led to a loss of tolerance while only loss of Chr3 trisomy impacted the MIC_{50} (Fig. 4e and Extended Data Fig. 8b). The tolerance of the concurrent aneuploid strains was higher than the additive tolerance of the mono-trisomy strains (indicated by red dashed line, Fig. 4e), suggesting that Chr3 and Chr6 act synergistically to confer multi-azole tolerance.

To test whether drug-related genes on Chr3 and Chr6 confer high tolerance when amplified, we engineered deletion mutants in the aneuploid strain. Chr3 encodes *MRR1*, a transcriptional regulator of the multidrug efflux pump encoded by *MDR1* on Chr6. Deletion of one copy of *MRR1* or one copy of *MDR1* from the concurrent aneuploid strain resulted in decreased tolerance (Fig. 4f). However, the tolerance was still higher than a loss of the extra copy of Chr3 or Chr6 from the concurrent aneuploid strain (Fig. 4f and Extended Data Fig. 8c). Similarly, over-expression of either *MRR1* or *MDR1* using a constitutive *tetO* promoter[48] in a euploid strain was not sufficient to reproduce the tolerance phenotypes of the concurrent aneuploid strain (Supplementary Note 4 and Extended Data Fig. 8d). Therefore, high copy numbers of *MRR1* and *MDR1* are both necessary but not sufficient for the high tolerance achieved by the concurrent aneuploid strain. Chr3 contains additional drug efflux pumps, encoded by *CDR1* and *CDR2*, therefore we quantified expression of *CDR1*, *CDR2*, *MRR1* and *MDR1* across the euploid and aneuploid strain backgrounds. Gene expression of all four genes was greater than or equal to the DNA copy number for all multi-azole tolerant aneuploid strains (Fig. 4g and Extended Data Fig. 8e). We conclude that multi-azole tolerance is associated with elevated expression of multiple drug efflux pumps and their transcriptional regulators.

Fluconazole selects for diverse genomic changes in vivo

To determine the frequency and effect of genomic changes that arise in the presence of three different concentrations of FLC in vivo, we applied our BFP/GFP system to a murine model of systemic infection. Five mice were infected intravenously with the Chr3 or Chr5 BFP/GFP

Fig. 5 | Colonies recovered from mice treated with FLC have increased fluorescence changes and ploidy variations. a, Schematic for mice infection. Mice were infected with Chr3 or Chr5 BFP/GFP reporter strains on day 0 via tail vein injection. Mice were treated with PBS or with FLC at 0.5, 2 or 5 mg kg^{-1} (FLC0.5, FLC2, FLC5) every day for 5 days. All mice were killed on day 6 and organs were collected for c.f.u.s and fungal cell recovery. Figure created with BioRender.com. **b**, Fungal burdens of mice kidneys that were infected with Chr3 BFP/GFP (left) or Chr5 BFP/GFP (right) strains. C.f.u.s were analysed on day 6 post infection. The lines and error bars indicate the median and interquartile range across all fungal c.f.u.s across mice from the same infection condition. Data were assessed for normality using a Shapiro–Wilk test and significant differences using one-way ANOVA with Dunnett's multiple comparisons test (two-sided). ****$P < 0.0001$, ***$P < 0.001$, *$P < 0.05$; exact *P* values are *0.0483, ***0.0001, 0.0001, 0.0002 and 0.0004, and ****<0.0001. **c**, Frequency of fluorescence changes among all colonies recovered from mice infected with Chr3 BFP/GFP (left) or Chr5 BFP/GFP (right) strains. The total number (*n*) of colonies recovered from mice and analysed for fluorescence phenotypes is indicated. **d**, WGS data of 12 representative colonies isolated from mice and selected on the basis of their BFP/GFP phenotypes, plotted as in Fig. 2. Boxes highlight the fluorescently tagged chromosome. **e**, Correlation of estimated ploidy and BFP/GFP fluorescence. Median G1 fluorescence of PI-stained cells (*x* axis) plotted according to the sum of the BFP and GFP fluorescent units (*y* axis) for FLC-treated mice samples. Samples from mice that had high frequency of fluorescence changes are presented here, with WGS samples labelled. Chr5_M1_FLC0.5 (purple squares), Chr3_M2_FLC2 (blue circles), Chr3_M1–5_FLC5 and Chr5_M4&M5_FLC5 (pink triangles), and PBS control Chr3_M1_PBS (grey hexagons). **f**, Ploidy analysis of four representative polyploid colonies with the diploid progenitor controls (>10,000 PI-stained cells). Dashed lines indicate G1 (2C) and G2 (4C) of the progenitors.

https://doi.org/10.1038/s41564-024-01795-7

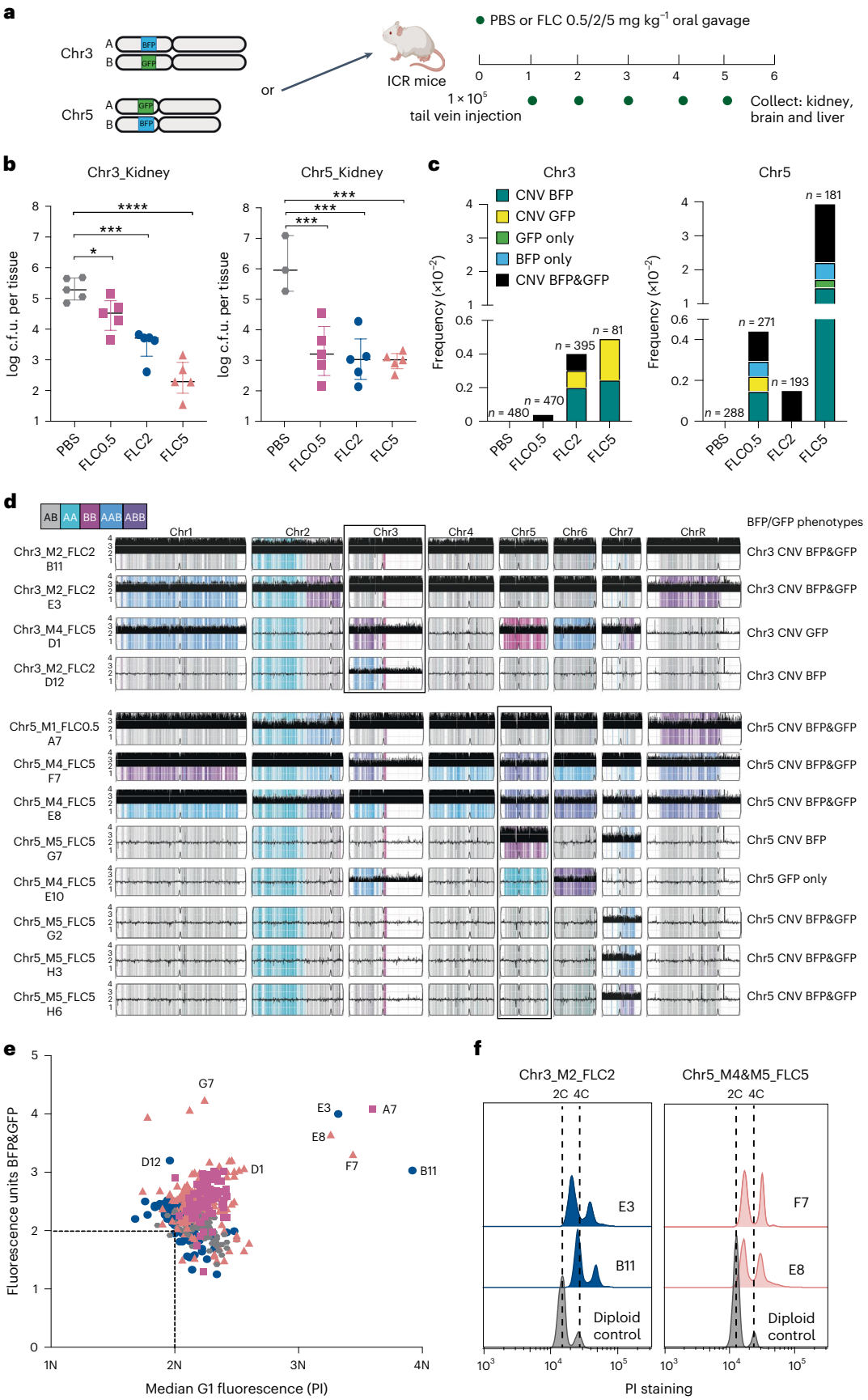

https://doi.org/10.1038/s41564-024-01795-7

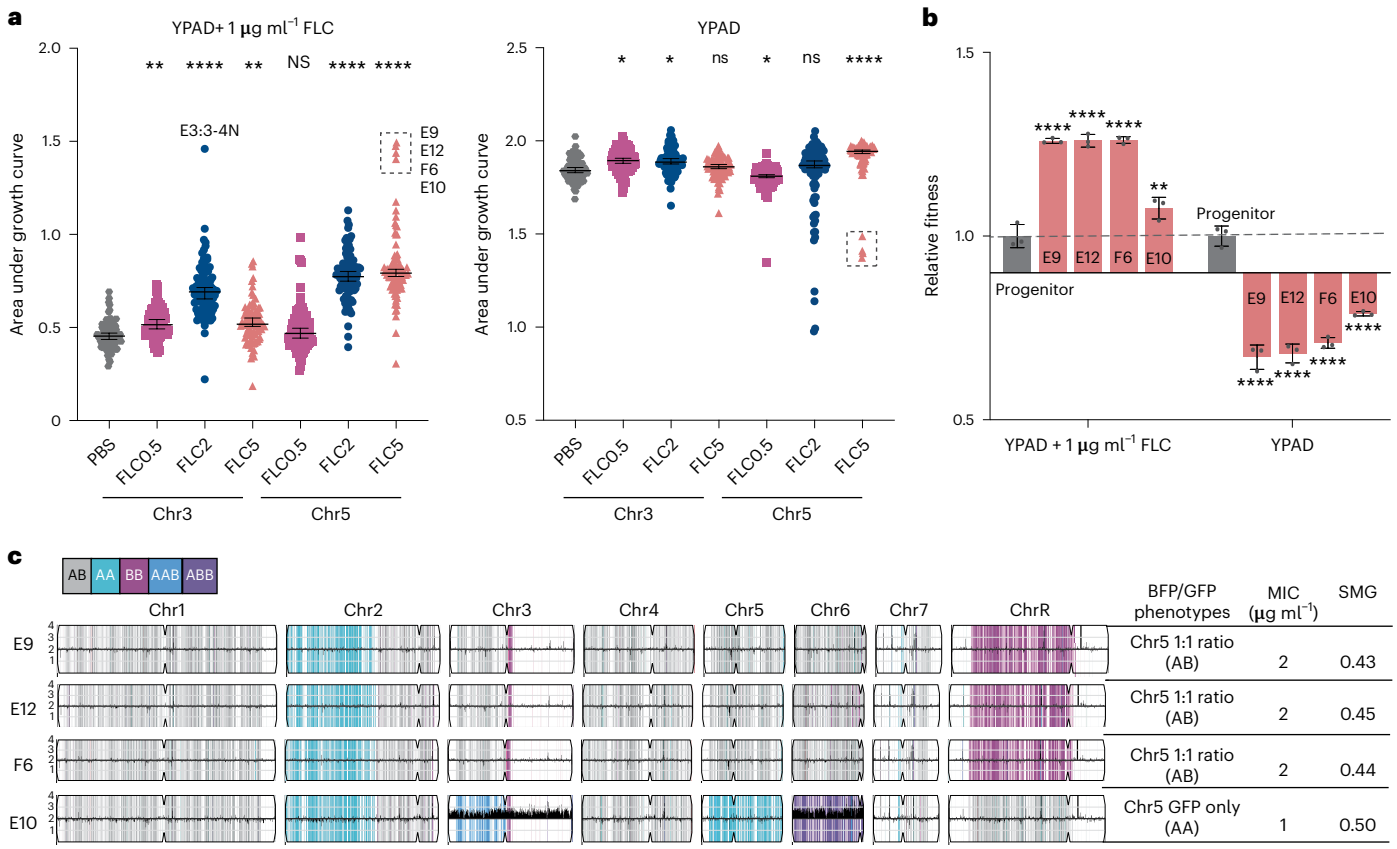

Fig. 6 | Samples recovered from mice treated with FLC have increased fitness in vitro. a, Growth rates in YPAD (right) and YPAD + 1 μg ml^{-1} FLC (left) from representative single colonies isolated from mice infected with Chr3 or Chr5 BFP/GFP strains and treated with PBS (grey) or 0.5 mg kg^{-1} (purple square), 2 mg kg^{-1} (blue circle) and 5 mg kg^{-1} FLC (pink triangle). Comparison was between colonies isolated from the PBS-treated and FLC-treated mice. Polyploid colony E3 is labelled. Dashed box indicates four diploid colonies that have increased growth in the presence of FLC (E9, E12, F6 and E10) and decreased growth in YPAD. Growth is indicated by the area under the growth curve after 48 h. The lines and error bars indicate the median and 95% confidence intervals across all single colonies from the same infection condition. **b**, Relative fitness determined for E9, E12, F6, E10 and the progenitor compared to the wild-type control. Data are mean ± s.e.m. calculated from 3 biological replicates. The dashed line indicates wild-type fitness. **a**,**b**, Data were assessed for normality using the Shapiro–Wilk test and significant differences using one-way ANOVA (**a**) or two-way ANOVA (**b**) followed by Dunnett's multiple comparisons test (two-sided). *$P < 0.05$, **$P < 0.01$, ****$P < 0.0001$; NS, $P > 0.05$; the exact P values are *0.0170, 0.0106 and 0.0121, **0.0018, 0.0013 and 0.0048, and ****<0.0001. **c**, WGS data plotted as in previous figures for colonies E9, E12, F6 and E10, with their FLC MIC (24 h) and SMG (48 h) values shown on the right.

progenitor strains for each condition. On days 1 through 5 post infection, mice were administered FLC at 0.5, 2 or 5 mg kg^{-1} by oral gavage and control mice received PBS (Fig. 5a). Six days post infection, all surviving mice (20/20 for Chr3 and 18/20 for Chr5) were killed and colony forming units (c.f.u.s) were recovered from kidney, liver and brain. No c.f.u.s were isolated from the liver under any conditions, and no c.f.u.s were isolated from the brain in any of the FLC conditions; therefore, we focused our analysis on the c.f.u.s recovered from the kidney. FLC significantly decreased the total c.f.u.s compared with no drug and there was a clear dose-dependent decrease in fungal burden with increasing FLC concentration for the Chr3 BFP/GFP strain, but no obvious dose response for the Chr5 BFP/GFP strain (Fig. 5b).

We performed flow cytometry analysis of the colonies isolated directly from the c.f.u. plates, up to 96 colonies per mouse. No BFP/GFP fluorescence changes on Chr3 or Chr5 were detected in ~800 colonies obtained from the 8 mice treated with PBS (Fig. 5c). In contrast, frequent fluorescence changes occurred on Chr3 and Chr5 in all the FLC-treated mice, with frequencies ranging from 0.042×10^{-2} to 3.95×10^{-2} (BFP/GFP CNV and LOH colonies per total colonies per mouse) among the different drug treatments (Fig. 5c). Chr3 and Chr5 exhibited distinct responses to different concentrations of FLC in mice, similar to in vitro. There was a bias for Chr5 CNV BFP (ABB), which was unstable in vitro[49], suggesting that this haplotype provides a fitness benefit in vivo in the presence of FLC (Fig. 5c, and Extended Data Fig. 7c and Supplementary Note 3)[49].

We selected 12 colonies with different fluorescent phenotypes from mice with high-frequency fluorescent changes (Chr3_FLC2/FLC5, Chr5_FLC0.5/FLC5) for WGS and found that 9/12 colonies exhibited the expected copy number changes on Chr3 or Chr5 (Fig. 5d,e and Supplementary Table 1). The remaining three colonies (G2, H3 and H6) had increased fluorescence of Chr5 BFP or GFP, but no Chr5 CNVs after overnight growth followed by WGS. These colonies probably lost the Chr5 CNV but were all trisomic for Chr7 which can promote *C. albicans* colonization of host organs (Fig. 5d)[50]. Interestingly, only whole-chromosome copy number changes were observed in the in vivo isolates, not segmental copy number changes (Fig. 5d). Overall, Chr3 and Chr5 have significantly increased copy number changes in the presence of FLC and have chromosome-specific responses under different FLC concentrations in vivo, similar to in vitro.

Polyploid colonies were recovered frequently from FLC-treated mice, reaching a frequency of 2.0×10^{-2} polyploid colonies per total colonies per mouse. These polyploid cells had ploidy ranging from triploid to tetraploid, were detected by increased fluorescence of both BFP and GFP (CNV BFP and GFP) and validated with propidium iodide (PI)-DNA staining (Fig. 5d–f and Extended Data Fig. 9a). These polyploid

cells exhibited chromosome instability ex vivo, resulting in new aneuploid karyotypes that correlated with decreased drug susceptibility (Supplementary Note 5 and Extended Data Fig. 9).

Fluconazole exposure in vivo selects for fitness advantages

Next, we quantified the growth of all mouse-derived colonies in the presence and absence of FLC. Overall, colonies from mice treated with FLC had increased growth in the presence of FLC compared with colonies isolated from mice treated with PBS (Fig. 6a). The highest growth in the presence of FLC was achieved by the polyploid colony E3 and four diploid colonies from mice treated with high concentrations of drug (2 or 5 mg kg^{-1} FLC) (Fig. 6a). In the absence of drug, these four colonies had poor growth relative to all mouse-derived colonies (Fig. 6a). This fitness trade-off was confirmed via a head-to-head competition experiment (Fig. 6b). All four colonies were diploid and three acquired LOH of ChrR resulting in ChrRBB (E9, E12 and F6), while the fourth colony E10 acquired LOH of Chr5AA and trisomy of Chr3 and Chr6 (Fig. 6c). Strikingly, FLC exposure in vitro and in vivo selected for some recurrent genotypes with significant fitness advantages. LOH resulting in haplotype ChrRBB was repeatedly identified in vivo and in vitro with other chromosome aneuploidies including from mice treated with high FLC (E9, E12, F6 and Chr5_FLC5_M1_A12) or low FLC in vitro (Extended Data Fig. 7). Similarly, cells with the Chr3 and Chr6 concurrent aneuploidies were isolated both in vivo and in vitro, and in all cases this concurrent aneuploidy correlated with elevated expression of *CDR1*, *CDR2*, *MRR1* and *MDR1* compared with the progenitor (Figs. 6c and 4g). This supports the idea that concurrent aneuploidies arise in vitro and in vivo and provide a selective advantage in the presence of drug.

Discussion

Genome copy number variants are pervasive and contribute substantially to evolution across all domains of life[51–54]; however, little is known about the rate and dynamics of these changes. We provide the first insight into the population dynamics of both CNV and LOH events in a fungal species during adaptation to antifungal drugs. Our results underscore that drug concentration dramatically alters selection for haplotype-specific CNV and LOH events both in vitro and in vivo, and that CNV and LOH events on different chromosomes arise at different frequencies. Copy number changes happen remarkably quickly, compete with other CNV or LOH lineages (clonal interference) and provide increased fitness. Under FLC selection, the frequency of cells with copy number changes increased more rapidly and resulted in a greater fitness advantage than copy number changes detected in other stress environments[39,55]. In addition, many CNVs decreased in frequency when drug selection was removed, while most LOH events maintained their frequency in the population in the absence of drug. This single-cell analysis provides quantification of the rate and dynamics of DNA copy number events in the presence of antifungal drug, distinguishing it from previous 'endpoint analyses' of copy number variants in *C. albicans*[12,20,23,25,31].

Concurrent copy number changes occurred on untagged chromosomes in nearly all in vitro and in vivo drug-evolved isolates. Chr3 and Chr6 concurrent aneuploidy was most frequent in our study, and has appeared during selection on FLC and posaconazole[31,56]. These findings highlight that concurrent chromosome copy number changes are pervasive and adaptive in the presence of azole drugs[31,56]. Furthermore, we dissected the synergistic effects of the Chr3 and Chr6 aneuploidies on drug susceptibility and provided molecular evidence that multiple genes on these chromosomes, when amplified together, are necessary to cause multi-azole tolerance. Concurrent aneuploidies such as Chr3 and Chr6 seem 'primed' to act synergistically in the presence of antifungal drug as they contain multiple, matched pairs of drug efflux pumps (*MDR1*, *CDR1*, *CDR2* and *ATM1*) and transcriptional regulators (*MRR1*, *CAP1* and *FLO8*)[57–59].

LOH is an important driver of phenotypic diversity in *C. albicans* including drug susceptibility and filamentation[14,17,30,60–62]. LOH resulting in homozygosis of a beneficial allele(s) can lead to phenotypic advantages[34,37,60,62,63]. We found recurrent haplotype-specific biases for Chr3, Chr6 and ChrR under drug selection, indicating that specific haplotypes contain beneficial allele(s) regulating drug susceptibility[17,37,62]. Recessive lethal alleles will dramatically alter haplotype-specific LOH frequencies. Several recessive lethal alleles have been characterized on Chr4B and Chr7B in the reference strain SC5314 (refs. 43,44). Here we found no evidence for recessive lethal alleles on Chr3, Chr5 or ChrR since homozygosis of both haplotypes was viable. Notably, Chr6 had the highest frequency of copy number changes among all untagged chromosomes in the presence of FLC; however, we never observed Chr6BB LOH (out of 122 WGS strains). More studies are needed to characterize the rate and effect of haplotype-specific events across diverse genetic backgrounds.

The BFP/GFP system enabled us to screen all viable cells obtained from mouse tissue for genomic changes in a high-throughput manner, eliminating marker selection steps used in previous mouse studies[50,64,65]. In general, increasing FLC concentrations decreased c.f.u.s; however, the colonies isolated from the FLC-treated mice had significantly higher frequency of copy number changes compared with the no-drug controls. The colonies isolated from the FLC-treated mice also had increased growth in the presence of FLC relative to the PBS-treated mice. This is presumably the first quantitative analysis of CNV and LOH events in the presence of antifungal in a mouse model of infection, and the dual-fluorescent reporter enabled us to detect amplification events indicative of polyploidization and attribute haplotype-specific drivers of drug resistance.

We detected a higher frequency of copy number changes in vitro than in vivo. Several factors probably contribute to this observation. First, we predict that in vitro, the *C. albicans* cells were exposed to a more constant and direct concentration of FLC than in vivo[6]. Second, the number of generations achieved in vivo was probably much smaller than the ~100 generations in vitro because of the single inoculum and shorter time frame of the in vivo experiments (6 days in vivo compared with 20 days in vitro), and different cell morphologies and growth dynamics (exponential vs linear growth) in vivo. Third, additional selective pressures that are not present in vitro, including immune cells, increased temperature (37 °C) and nutrient/oxidative/nitrosative stress, are probably impacting the emergence of copy number changes in vivo[14,15,42]. These fitness trade-offs may limit the adaptive trajectories available to *C. albicans* in vivo. Nonetheless, we found similar, recurrent genotypes in vivo and in vitro that correlated with increased fitness in the presence of FLC, including polyploidy, ChrR LOH and concurrent trisomy of Chr3 and Chr6.

In summary, this study used a dual-fluorescent reporter system to rapidly quantify diverse genomic copy number changes that arise in *C. albicans* cells during adaptation to antifungal drug. We identified haplotype-specific and recurrent copy number changes that correlated with increased fitness in the presence of drug. We highlight the importance of LOH, polyploidy and concurrent aneuploidy during adaptation to drug, both in vitro and in vivo. The dual-fluorescent reporter is highly adaptable, and this report lays important groundwork for future studies aimed at uncovering the rate and dynamics of genome instability across diverse species and stress environments.

Methods

Yeast isolates and culture conditions

All strains used in this study are listed in Supplementary Table 1, including the Chr3 and Chr5 BFP/GFP progenitors, FLC-evolved single colonies, FACS-isolated single cells, mice-evolved single colonies, concurrent aneuploid evolved single colonies and engineered over-expressing strains. Strains were stored at −80 °C in 20% glycerol. Isolates were grown at 30 °C in YPAD medium (peptone, yeast extract,

2% dextrose and 2% agar for plates) supplemented with 40 μg ml^{-1} adenine and 80 μg ml^{-1} uridine.

Strain construction

All *C. albicans* strains in this study were generated in the Sn152 background and then made prototrophic[66]. All strains were constructed by lithium acetate transformation using PCR products with at least 140 bp of homology to the target locus. All primers used in this study are listed in Supplementary Table 2.

Fluorescent BFP/GFP reporter strains. The positions for the BFP/GFP constructs on Chr3 or Chr5 were selected using the following criteria: (1) intergenic regions greater than 3 kb, (2) greater than 100 kb away from any telomere sequence, (3) 100 kb away from the centromere and (4) position excludes repetitive sequences identified in ref. 11.

GFP-ARG4 and *BFP-HIS1* under the *TDH3* promoter were amplified via PCR from plasmids ECC596 and ECC727, respectively, generous gifts from Melanie Legrand[40]. Primer sets 1415 + 1416 and 1425 + 1426 were used for Chr3 and Chr5, respectively. *GFP-ARG4* or *BFP-HIS1* were first transformed into background strain Sn152 at intergenic regions; Chr3: 648571–651482 or Chr5: 404709–407546. Transformants were validated by PCR for both left (Chr3: *GFP-ARG4/BFP-HIS1* 1398 + 1388/1398 + 1393, Chr5: *GFP-ARG4/BFP-HIS1* 1427 + 1388/1427 + 1393) and right integrations (Chr3: *GFP-ARG4/BFP-HIS1* 1391 + 1399, Chr5: *GFP-ARG4/BFP-HIS1* 1391 + 1429). Transformants were PCR tested for the absence of wild-type intergenic regions using primers 1398 + 1401 (Chr3) or 1427 + 1428 (Chr5). The correct transformants with *BFP-HIS1* were then used as the background for second-round transformations which were done by adding the *GFP-ARG4* into mono-BFP at the same locus of Chr3 or Chr5 but the second alleles. Likewise, the correct transformants with *GFP-ARG4* were then used as the background for second-round transformations which were done by adding the *BFP-HIS1* into mono-GFP at the same locus of Chr3 or Chr5 but the second alleles. Transformants were again validated by PCR for left integrations using the same primers as above. For right integration, different primers were used to confirm the insertion at the second alleles (Chr3: *GFP-ARG4/BFP-HIS1* 1389 + 1399/1392 + 1399, Chr5: *GFP-ARG4/BFP-HIS1* 1389 + 1429/1392 + 1429). Correct transformants with both *BFP-HIS1* and *GFP-ARG4* at the correct positions were complemented with *LEU2*, which was amplified via PCR from SC5314 (1557 + 1559). *LEU2* integration was confirmed with primers 1558 + 1560/1560 + 1561. The prototrophic, dual-fluorescent reporter strains (*BFP-HIS1*, *GFP-ARG4* and *LEU2)* were validated with whole-genome sequencing and confirmed by flow cytometry to be diploid.

***MDR1* or *MRR1* over-expression strains.** The tetO promoter replacement construct was PCR amplified from pLC605, a generous gift from Leah E. Cowen[48]. Primer sets 1283 + 1284 and 1720 + 1721 were used for *MDR1* and *MRR1* tetO constructs, respectively. The tetO constructs were then transformed into the wild-type background (Sn152). NAT-resistant transformants were PCR verified for integration of the tetO promoter at the *MDR1* or *MRR1* locus using the primers 1285 + 1176/1179 + 1286 or 1716 + 1176/1177 + 1717. Transformants were PCR tested for the absence of a wild-type promoter of *MDR1* or *MRR1* using the primers 1285 + 1286 or 1716 + 1717. Transformants were validated using WGS.

Deletion of *MRR1* or *MDR1*. Heterozygous deletion of *MRR1* or *MDR1* was performed in the concurrent aneuploid strain (Chr3_FLC8_L12_S5; Supplementary Table 1). Deletion mutants were constructed by lithium acetate transformation using PCR products with at least 140 bp of homology to the target locus. The FLIP-NAT construct was PCR amplified from the plasmid pJK863 (ref. 67) using primer sets 1720 + 2000 (*MDR1*) and 1283 + 1997 (*MRR1*) and transformed into concurrent aneuploid background strains. NAT-resistant transformants were PCR screened for correct integration of the FLIP-NAT construct at the *MRR1 or MDR1* locus using primer pairs 1998 + 1045 (*MRR1*) or 1716 + 1045 (*MDR1*) (left of integration) and 1636 + 1999 (*MRR1*) or 1636 + 2001 (*MDR1*) (right of integration). All correct transformants are listed in Supplementary Table 1.

Verification of BFP/GFP integration using whole-genome sequencing

To verify the correct integration of BFP and GFP constructs, a new reference genome ('BFP/GFP reference genome') was created from the SC5314 A21 reference genome plus two additional contigs composed of the target constructs (*GFP-ARG4* and *BFP-HIS1)*. Transformants were aligned to the BFP/GFP reference genome and checked for correct integration via read depth at the new *GFP-ARG4* and *BFP-HIS1* contigs, and identification of discordant reads where mates mapped to the insert sequence (*BFP-HIS1*/*GFP-ARG4*) and at the integration site (on Chr3 or Chr5).

In vitro evolution experiment

BFP/GFP-tagged progenitors AMS5178 (Chr3) and AMS5192 (Chr5) were plated on YPAD agar and incubated for 24 h at 30 °C. Twelve single colonies from each strain were selected and inoculated in liquid YPAD in deep-well 96-well plates. Plates were sealed with BreathEASIER (Electron Microscope Sciences) tape and cultured for 16–18 h at 30 °C and 220 r.p.m. From each of the 12 single-colony lineages, a 1:1,000 dilution was made into four culture conditions: (1) YPAD with 0 μg ml^{-1} FLC, (2) YPAD with 1 μg ml^{-1} FLC, (3) YPAD with 4 μg ml^{-1} FLC and (4) YPAD with 8 μg ml^{-1} FLC, again in deep-well 96-well plates. The MIC_{50} for the BFP/GFP reporter strains was 0.5 μg ml^{-1} FLC, therefore 1 μg ml^{-1} FLC represented a near-MIC concentration, and 4 and 8 μg ml^{-1} FLC represented supra-MIC concentrations[23,25]. Each progenitor was on a separate 96-well plate and each environmental condition was separated with a blank row. Plates were sealed with BreathEASIER tape and cultured at 30 °C and 220 r.p.m. At each 48 h timepoint, cells were resuspended and transferred via 1:1,000 dilution to fresh YPAD medium containing the designated concentration of FLC, for 10 total transfers (P1–P10). Starting at P11 and continuing to P15, no FLC was added, and all populations were cultured in YPAD with 0 μg ml^{-1} FLC, with 1:1,000 dilutions every 48 h (Extended Data Fig. 2a). At each transfer, cells were collected for storage at −80 °C.

Flow cytometry sampling and analysis

Before flow cytometry analysis, all isolates were inoculated in YPAD from frozen stocks and incubated for 12–16 h at 30 °C and 220 r.p.m. Cultures were diluted in PBS and at least 10,000 singlets were gated and analysed for each sample using a Cytek Aurora flow cytometer (R0021). Lasers (405 nm) were used to excite the BFP proteins and 458/15 filters were used to detect the BFP emission signals. Lasers (488 nm) were used to excite the GFP proteins and 508/20 filters were used to detect the GFP emission signals. Data were analysed using FlowJo (https://www.flowjo.com/solutions/flowjo/downloads) (v.10.8.1). The 12 lineages evolved in 0 μg ml^{-1} were used as the 1:1 ratio (BFP:GFP) control for each passage, eliminating growth condition and cytometer variation effects on fluorescence changes (Extended Data Fig. 2b). Non-fluorescent, mono-fluorescent and dual-fluorescent controls were used for gating. We removed doublets (FSC-A vs FSC-H) and drew gates to fit the non-fluorescent/dead cells (BFP− GFP−), mono-fluorescent BFP (BFP+ GFP−), mono-fluorescent GFP (BFP− GFP+) and the dual-fluorescent cells (BFP+ GFP+) (Extended Data Fig. 1c–e). Within the dual-fluorescent gate, BFP/GFP progenitor strains with only one copy of both BFP and GFP were used to generate a 1:1 ratio (BFP vs GFP) gate (Extended Data Fig. 1e). Dual-fluorescent cells that were outside this 1:1 gate were further gated as CNVs due to increased fluorescence of BFP, GFP or both BFP and GFP (Extended Data Fig. 1e,f). The proportions of each subpopulation were calculated and normalized by the total viable cell count and used to generate the stacked plots with R programming language (v.4.1.2) (Figs. 1 and 2).

Quantification of the dynamics of subpopulations with fluorescence changes

To quantify the dynamics of subpopulations with fluorescence changes, we defined T_{up} and S_{up} as described previously[39]. Using the defined gates, we determined the abundance of subpopulations with varied fluorescent phenotypes at every passage. T_{up} is the generation at which subpopulations with fluorescence changes were initially detected. By quantifying the fluorescence changes of 24 YPAD control lineages from P0 (12 h in YPAD), we defined a false positive threshold of 2% out of 10,000 single-cell events. We designated T_{up} once the subpopulation with fluorescent change surpassed this threshold. T_{peak} was designated once the subpopulation with fluorescence changes reached the maximum frequency in the population during the initial expansion. S_{up} is the rate of increase in the subpopulations with fluorescence changes per generation during the initial expansion, which is an approximation for the relative average fitness of subpopulations with fluorescence changes. S_{down} is also defined here to calculate the rate of decrease in the subpopulation with fluorescence changes per generation after the drug was removed. To calculate S_{up}/S_{down}, we plotted the natural log of the ratio of the proportion of cells with a certain fluorescence change and the rest of the population against time and calculated the linear fit during initial population expansion/decrease. S_{up}/S_{down} is the slope of the linear fit during initial population expansion/decrease (Supplementary Table 3).

Fluorescence-activated cell sorting

BFP/GFP-tagged progenitor AMS5178 (Chr3) and AMS5192 (Chr5) strains were plated on YPAD agar from frozen stocks and incubated for 24 h at 30 °C. At least three single colonies of each strain were selected and inoculated into 50 ml of YPAD and grown for 36 h at 30 °C and 220 r.p.m. These cultures were diluted in PBS + 5 mM EDTA and then passed through a cell strainer (70 µm) for FACS using a BD FACSAria II analyser (P07800142). After setting up the gates (Extended Data Fig. 1c–e), single cells with the targeted fluorescent profile (BFP− GFP+ or BFP+ GFP−) (Fig. 3a) were collected into individual wells of a 96-well plate containing YPAD. Collected cells were grown for 48 h at 30 °C in a humidified chamber, then saved in frozen stocks. All collected samples were re-analysed on a Cytek Aurora flow cytometer (R0021) to confirm their fluorescent phenotypes. In total, 26 samples with target fluorescent phenotypes were selected for whole-genome sequencing to validate genotypes of LOH cells (Extended Data Fig. 4).

Single-colony selection

Selected FLC-evolved lineages were patched onto YPAD agar plates supplemented with 1 µg ml^{-1} FLC to help stabilize the genomic changes. After incubation at 30 °C for 24–36 h, 12–24 colonies were randomly selected and cultured in liquid YPAD for 12–16 h before flow cytometry analysis (Extended Data Fig. 5 and Fig. 4). BFP/GFP profiles of single colonies 1–12 (S1–12) are shown in Extended Data Fig. 5b, and the distribution of single colonies closely matches the population fraction of Chr3_FLC_L5 (Extended Data Fig. 5a,b).

Relative fitness assay

Isolates were inoculated in YPAD from frozen stocks and incubated for 16 h at 30 °C and 220 r.p.m. Cultures were diluted in fresh 1% dextrose[23,68] YPAD to a final optical density (OD_{600}) of 0.01. Normalized cultures from two different isolates were then combined at 1:9 (sample of interest:WT-control), and 20 µl of this combined culture was added to a 96-well plate containing 180 µl of 1% dextrose YPAD supplemented with or without FLC (initial OD_{600}, N_0 = 0.001). Cells were incubated at 30 °C in a BioTek Epoch 2 microplate spectrophotometer with double-orbital (237 r.p.m) shaking. OD_{600} readings were taken every 15 min for 48 h to monitor cell growth, as well as at the endpoint. A volume of 20 µl culture was removed from one of the triplicates for flow cytometry at different time points: 12, 16, 24 and 48 h. Cultures were diluted in PBS and 10,000 singlets were gated and analysed at each timepoint using a Cytek Aurora flow cytometer (R0021). After 16 h, populations reached the stationary phase and OD_{600} was ~1.3 (N_t), therefore there were a total of 10 generations for the competition assay, estimated using equation generations = $[\log_{10}(N_t/N_0)]/0.3$. At different time points, proportions of the sample interest were indicated by the proportion of cells with fluorescence, while WT-control were indicated by non-fluorescent cells. All competitive assays were conducted in three independent replicates. Relative fitness was estimated using natural log regression analysis of the proportions of the sample of interest and the WT-control against the generations (10 generations): ln (proportion of sample of interest / proportion of WT-control) / generations.

Microdilution MIC and SMG assays

Antifungal drug susceptibilities were determined using a microwell broth dilution assay[22]. Isolates were inoculated in YPAD from frozen stocks and incubated for 16–18 h at 30 °C and 220 r.p.m. Cultures were diluted in fresh 1% dextrose[23,68] YPAD to a final OD_{600} of 0.01. A volume of 20 µl of this dilution was added to 180 µl of 1% dextrose YPAD media containing either a 2-fold serial dilution of drug or a no-drug control. Drug concentrations ranged from 0.5 µg ml^{-1} to 256 µg ml^{-1} FLC, and 0.0625 µg ml^{-1} to 32 µg ml^{-1} itraconazole or voriconazole. Triplicates of each isolate were set up using flat-bottom 96-well plates and incubated in a humidified chamber at 30 °C. Cells were resuspended at the 24 h and 48 h time points, and OD_{600} readings were taken using a BioTek Epoch 2 microplate spectrophotometer. The MIC_{50} of each strain was determined to be the drug concentration at which ≥50% of growth was inhibited when compared with the no-drug control at 24 h post inoculation. The SMG was measured as the average growth (OD_{600}) above the MIC_{50} when standardized to the no-drug control at 48 h post inoculation.

Growth curve

Isolates were inoculated in YPAD from frozen stocks and incubated for 16 h at 30 °C and 220 r.p.m. Cultures were diluted in fresh 1% dextrose YPAD to a final OD_{600} of 0.01. A volume of 20 µl of this dilution was added to a 96-well NUNC plate containing 180 µl of 1% dextrose YPAD supplemented with or without drug and incubated at 30 °C in a BioTek Epoch 2 microplate spectrophotometer with double-orbital (237 r.p.m) shaking. OD_{600} readings were taken every 15 min for 48 h. Every isolate inoculation was conducted in three independent replicates.

Ploidy analysis

Cells were prepared as described previously[69]. Isolates were inoculated in YPAD from frozen stocks and incubated overnight at 30 °C and 220 r.p.m to a cell density of 1×10^7 cells per ml. Cultures were gently spun down at 3,000 r.p.m for 3 min and the supernatant was removed. Cell pellets were resuspended in 70% ethanol, then washed twice with 50 mM sodium citrate. Following washing, cells were spun down and resuspended in 50 mM sodium citrate containing 0.5 mg ml^{-1} RNase A. Cells were treated with RNase A at 37 °C for at least 2 h, then stained with 25 µg ml^{-1} PI at 37 °C in the dark overnight. Samples were diluted in 50 mM sodium citrate and at least 10,000 singlets were analysed using a Cytek Aurora flow cytometer (R0021). The 488 nm lasers were used to excite the PI-staining and 618/24 filters were used to detect the PI-staining emission signals. Unstained cells were used as negative control. The diploid progenitor control was used to define G1 (1C) and G2 (2C) peaks. Data were analysed using FlowJo (https://www.flowjo.com/solutions/flowjo/downloads) (v.10.8.1).

Reverse transcriptase qPCR

Strains were inoculated into 5 ml YPAD and grown overnight for 16–18 h at 30 °C with shaking. To maintain the Chr3 and Chr6 trisomies, 1 µg ml^{-1} FLC was added to the overnight cultures. Cultures were then diluted

1:20 by transferring 250 µl of culture into 5 ml YPAD (1% dextrose) with 1 µg ml^{-1} FLC and grown at 30 °C for 4 h with shaking. RNA was prepared according to manufacturer instructions for the MasterPure Yeast RNA Purification kit (Epicentre). Removal of contaminating DNA was performed using DNase (Epicentre) followed by heat inactivation of DNase. Complementary (c)DNA was prepared using the LunaScript RT Master Mix kit (primer-free) (New England Biolabs) according to manufacturer instructions, with oligo dT primers and 100 ng of RNA. A no-RT control reaction was also performed for each strain using oligo dT primers according to manufacturer instructions for LunaScript RT Master Mix kit (primer-free). cDNA was then diluted 1:1 with nuclease-free water for qPCR measurement. Real-time qPCR was conducted to measure cDNA using the Luna Universal qPCR master mix (New England Biolabs) according to manufacturer instructions. Using a CFX Connect Real-Time PCR Detection System and Bio-Rad CFX Maestro software (v.2.0) to determine *C*q values, expression was calculated as the amount of cDNA from the gene of interest relative to the amount of *TEF1* cDNA in the same sample. All primers used in this study are listed in Supplementary Table 2.

Illumina whole-genome sequencing

Genomic DNA was isolated using phenol-chloroform extraction as described previously[8]. Libraries were prepared using the Illumina DNA Prep kit and IDT 10 bp UDI indices and sequenced on an Illumina NextSeq 2000 system, producing 2 × 151 bp reads. Demultiplexing, quality control and adapter trimming were performed with bcl-convert (https://support.illumina.com/sequencing/sequencing_software/bcl-convert.html)(v.3.9.3). Adapter and quality trimming were performed with BBDuk (BBTools v.38.94)[70]. Trimmed reads were aligned to the *C. albicans* reference genome (SC5314_version_A21-s02-m09-r08) using BWA-MEM (v.0.7.17) with default parameters[71,72]. Aligned reads were sorted, duplicate reads were marked and the resulting BAM file was indexed with Samtools (v.1.10)[73]. The quality of trimmed FASTQ and BAM files was assessed for all strains with FastQC (v.0.11.7), Qualimap (v.2.2.2-dev) and MultiQC (v.1.16)[74–76].

Visualization of whole-genome sequencing data

Chromosomal copy number changes were visualized using the Yeast Mapping Analysis Pipeline (YMAP v.1.0)[77]. Aligned bam files were uploaded to YMAP and read depth was determined and plotted as a function of chromosome position using the reference genome *C. albicans* SC5314 (A21-s02-m09-r08). Read depth was corrected for GC-content and chromosome-end bias. WGS data were plotted as the $\log_2$ ratio and converted to chromosome copy number (*y* axis, 1–4 copies) as a function of chromosome position (*x* axis, Chr1–ChrR) using YMAP[77]. The baseline chromosome copy number (ploidy) was determined by flow cytometry. Haplotypes are indicated by colour: grey is heterozygous AB, magenta is homozygous B and cyan is homozygous A.

Identification of whole-chromosome and segmental LOH events

Preliminary identification of LOH events was conducted using aligned Illumina reads and the YMAP plots generated above. YMAP plots for each strain were visually compared with the reference genome *C. albicans* SC5314 (A21-s02-m09-r08) to look for regions that underwent homozygosis, on the basis of heterozygosity in the progenitor at the same region. Approximate LOH boundaries were identified from YMAP GBrowse allele ratio tracks and confirmed by visual inspection in IGV (IGV v.2.8.2)[78]. Several gene conversion events involving just the GFP or BFP reporter were detected: GFP-only or BFP-only cells were detected by flow cytometry, but WGS analysis indicated that the tagged chromosome was heterozygous. We confirmed that LOH occurred only at the tagged locus by quantifying the average read depth of the BFP/GFP contigs in the BFP/GFP reference genome. *BFP-HIS1* and *GFP-ARG4* contigs are provided in source data.

Variant calling

De novo variant calling and preliminary filtering were performed with Mutect2 and FilterMutectCalls (GATK v.4.1.2), both with default parameters[79]. Variant calling was run separately for 3 groups of strains corresponding to the different progenitors. The first group called the SC5314 progenitor as 'normal' and the BFP/GFP-tagged strains AMS5178 and AMS5192 as 'tumour'. The second group called AMS5178 as 'normal' and AMS5178-derived strains as 'tumour'. The third group called AMS5192 as 'normal' and AMS5192-derived strains as 'tumour'. Additional VCF filtering was performed with bcftools (v.1.17)[73]. Individual VCF files were subset to remove the progenitor strain and filtered for calls with a quality status of 'PASS'. A merged VCF file was created for each progenitor group. Merged VCF files were subset to exclude repeat regions (as marked in the SC5314 A21-s02-m09-r08 GFF) and 5,000 bp subtelomeric regions, and additional hard filtering was performed (minimum of 5 supporting reads, at least one supporting read in both forward and reverse direction, minimum alternate allele frequency of 0.2 for diploid, single-colony cultures, minimum alternate allele frequency of 0.05 for polyploids and population cultures). Identical variants found in at least half of all progeny were considered to be present in the progenitor strain and were removed[23]. Variants were annotated with SnpEff (v.5.0e; database built from SC5314 v.A21-s02-m09-r08, with alternate yeast nuclear codon table) and visually verified in IGV[80,81]. Verified variants were compiled into Supplementary Table 4 using GATK VariantsToTable and bcftools query.

Mouse model of candidiasis

The animal experiments were performed using 6-week-old male outbred CD-1 mice. *C. albicans* progenitor strains AMS5178 (Chr3) and AMS5192 (Chr5) were inoculated in YPAD and incubated for 16 h at 30 °C. On day 0, immunocompetent CD-1 mice were injected with 4×10^4 (AMS5178) or 1×10^5 (AMS5192) cells. Starting on day 1, mice were administered FLC at 0.5, 2 or 5 mg kg^{-1} by gavage. Control mice received PBS. The mice were weighed every day to determine the FLC dose. Drug treatment continued for 5 days. On day 6, mice were killed and tissues including kidney, brain and liver were collected. These tissues were weighed, homogenized and quantitatively cultured for c.f.u.s counting and fungal cell recovery.

Statistical analyses

GraphPad Prism (v.10.11) for macOS was used to generate graphical representations of numerical data. Inferential statistical tests were performed using GraphPad Prism. The data sets were assessed for normality with a Shapiro–Wilk test and differences between control and strains with copy number changes were calculated using one-way or two-way ANOVA (details provided in figure legends). ANOVA tests were followed by Dunnett's or Šídák's multiple comparisons test. Dunnett's test was selected when comparing more than one data set to the control. Šídák's test was selected for comparisons between only two data sets. Differences were considered statistically significant if $P < 0.05$.

Ethics statement

All animal work was approved by the Institutional Animal Care and Use Committee of the Lundquist Institute for Biomedical Innovation at Harbor-UCLA Medical Center under animal welfare assurance number D16-00213. The mice were housed at 20 °C on a 12 h light/dark cycle in ambient humidity.

Reporting summary

Further information on research design is available in the Nature Portfolio Reporting Summary linked to this article.

Data availability

All whole-genome sequences (FASTQ files) are available in the Sequence Read Archive repository under BioProject PRJNA973218. All BioSample

numbers are listed in Supplementary Table 1. All the flow cytometry raw data (.fcs files) are available at the Data Repository of the University of Minnesota (https://doi.org/10.13020/pg0z-ag23)[82]. All the strains used in this study are available upon request. Source data are provided with this paper.

Code availability

All computational scripts used for stacked plots and whole-genome sequence alignment and variant calling are publicly available through the Selmecki Lab GitHub page (https://github.com/selmeckilab)[83].

References

1. Pfaller, M. A., Diekema, D. J., Turnidge, J. D., Castanheira, M. & Jones, R. N. Twenty years of the SENTRY antifungal surveillance program: results for *Candida* species from 1997–2016. *Open Forum Infect. Dis.* **6**, S79–S94 (2019).
2. Pfaller, M. A. Antifungal drug resistance: mechanisms, epidemiology, and consequences for treatment. *Am. J. Med.* **125**, S3–S13 (2012).
3. Andes, D. R. et al. Impact of treatment strategy on outcomes in patients with candidemia and other forms of invasive candidiasis: a patient-level quantitative review of randomized trials. *Clin. Infect. Dis.* **54**, 1110–1122 (2012).
4. Cowen, L. E. The evolution of fungal drug resistance: modulating the trajectory from genotype to phenotype. *Nat. Rev. Microbiol.* **6**, 187–198 (2008).
5. Perea, S. et al. Prevalence of molecular mechanisms of resistance to azole antifungal agents in *Candida albicans* strains displaying high-level fluconazole resistance isolated from human immunodeficiency virus-infected patients. *Antimicrob. Agents Chemother.* **45**, 2676–2684 (2001).
6. Schiave, L. A. et al. Fluconazole levels in serum and cerebrospinal fluid according to daily dosage in patients with cryptococcosis and other fungal infections. *Braz. J. Infect. Dis.* **22**, 11–15 (2018).
7. Sionov, E., Chang, Y. C., Garraffo, H. M. & Kwon-Chung, K. J. Heteroresistance to fluconazole in *Cryptococcus neoformans* is intrinsic and associated with virulence. *Antimicrob. Agents Chemother.* **53**, 2804–2815 (2009).
8. Selmecki, A., Forche, A. & Berman, J. Aneuploidy and isochromosome formation in drug-resistant *Candida albicans*. *Science* **313**, 367–370 (2006).
9. Selmecki, A., Gerami-Nejad, M., Paulson, C., Forche, A. & Berman, J. An isochromosome confers drug resistance in vivo by amplification of two genes, ERG11 and TAC1. *Mol. Microbiol.* **68**, 624–641 (2008).
10. Todd, R. T. & Selmecki, A. Expandable and reversible copy number amplification drives rapid adaptation to antifungal drugs. *Elife* **9**, e58349 (2020).
11. Todd, R. T., Wikoff, T. D., Forche, A. & Selmecki, A. Genome plasticity in *Candida albicans* is driven by long repeat sequences. *Elife* **8**, e45954 (2019).
12. Burrack, L. S., Todd, R. T., Soisangwan, N., Wiederhold, N. P. & Selmecki, A. Genomic diversity across *Candida auris* clinical isolates shapes rapid development of antifungal resistance in vitro and in vivo. *mBio* **13**, e0084222 (2022).
13. Poláková, S. et al. Formation of new chromosomes as a virulence mechanism in yeast *Candida glabrata*. *Proc. Natl Acad. Sci. USA* **106**, 2688–2693 (2009).
14. Forche A. et al. Stress alters rates and types of loss of heterozygosity in *Candida albicans*. *mBio* https://doi.org/10.1128/mbio.00129-11 (2011).
15. Harrison, B. D. et al. A tetraploid intermediate precedes aneuploid formation in yeasts exposed to fluconazole. *PLoS Biol.* **12**, e1001815 (2014).
16. Cowen, L. E. et al. Evolution of drug resistance in experimental populations of *Candida albicans*. *J. Bacteriol.* **182**, 1515–1522 (2000).
17. Hirakawa, M. P. et al. Genetic and phenotypic intra-species variation in *Candida albicans*. *Genome Res.* **25**, 413–425 (2015).
18. Chibana, H., Beckerman, J. L. & Magee, P. T. Fine-resolution physical mapping of genomic diversity in *Candida albicans*. *Genome Res.* **10**, 1865–1877 (2000).
19. Tso, G. H. W. et al. Experimental evolution of a fungal pathogen into a gut symbiont. *Science* **362**, 589–595 (2018).
20. Forche, A., Magee, P. T., Selmecki, A., Berman, J. & May, G. Evolution in *Candida albicans* populations during a single passage through a mouse host. *Genetics* **182**, 799–811 (2009).
21. Pfaller, M. A. et al. Variations in fluconazole susceptibility and electrophoretic karyotype among oral isolates of *Candida albicans* from patients with AIDS and oral candidiasis. *J. Clin. Microbiol.* **32**, 59–64 (1994).
22. Rosenberg, A. et al. Antifungal tolerance is a subpopulation effect distinct from resistance and is associated with persistent candidemia. *Nat. Commun.* **9**, 2470 (2018).
23. Todd, R. T. et al. Antifungal drug concentration impacts the spectrum of adaptive mutations in *Candida albicans*. *Mol. Biol. Evol.* **40**, msad009 (2023).
24. Berman, J. & Krysan, D. J. Drug resistance and tolerance in fungi. *Nat. Rev. Microbiol.* **18**, 319–331 (2020).
25. Yang, F. et al. Antifungal tolerance and resistance emerge at distinct drug concentrations and rely upon different aneuploid chromosomes. *mBio* **14**, e00227-23 (2023).
26. Sionov, E., Chang, Y. C. & Kwon-Chung, K. J. Azole heteroresistance in *Cryptococcus neoformans*: emergence of resistant clones with chromosomal disomy in the mouse brain during fluconazole treatment. *Antimicrob. Agents Chemother.* **57**, 5127–5130 (2013).
27. Ford, C. B. et al. The evolution of drug resistance in clinical isolates of *Candida albicans*. *Elife* **4**, e00662 (2015).
28. Mount, H. O. et al. Global analysis of genetic circuitry and adaptive mechanisms enabling resistance to the azole antifungal drugs. *PLoS Genet.* **14**, e1007319 (2018).
29. Bergin Sean, A. et al. Systematic analysis of copy number variations in the pathogenic yeast *Candida parapsilosis* identifies a gene amplification in RTA3 that is associated with drug resistance. *mBio* **13**, e01777-22 (2022).
30. Selmecki, A. M., Dulmage, K., Cowen, L. E., Anderson, J. B. & Berman, J. Acquisition of aneuploidy provides increased fitness during the evolution of antifungal drug resistance. *PLoS Genet.* **5**, e1000705 (2009).
31. Kukurudz, R. J. et al. Acquisition of cross-azole tolerance and aneuploidy in *Candida albicans* strains evolved to posaconazole. *G3* **12**, jkac156 (2022).
32. Hill, J. A., Ammar, R., Torti, D., Nislow, C. & Cowen, L. E. Genetic and genomic architecture of the evolution of resistance to antifungal drug combinations. *PLoS Genet.* **9**, e1003390 (2013).
33. Gerstein, A. C. & Berman, J. *Candida albicans* Genetic background influences mean and heterogeneity of drug responses and genome stability during evolution in fluconazole. *mSphere* **5**, e00480-20 (2020).
34. Coste, A. T., Karababa, M., Ischer, F., Bille, J. & Sanglard, D. TAC1, transcriptional activator of CDR genes, is a new transcription factor involved in the regulation of *Candida albicans* ABC transporters CDR1 and CDR2. *Eukaryot. Cell* **3**, 1639–1652 (2004).
35. Morschhäuser, J. et al. The transcription factor Mrr1p controls expression of the MDR1 efflux pump and mediates multidrug resistance in *Candida albicans*. *PLoS Pathog.* **3**, e164 (2007).

36. Schubert, S. et al. Regulation of efflux pump expression and drug resistance by the transcription factors Mrr1, Upc2, and Cap1 in *Candida albicans*. *Antimicrob. Agents Chemother.* **55**, 2212–2223 (2011).
37. Dunkel, N., Blass, J., Rogers, P. D. & Morschhäuser, J. Mutations in the multi-drug resistance regulator MRR1, followed by loss of heterozygosity, are the main cause of MDR1 overexpression in fluconazole-resistant *Candida albicans* strains. *Mol. Microbiol.* **69**, 827–840 (2008).
38. Spealman, P., De, T., Chuong, J. N. & Gresham, D. Best practices in microbial experimental evolution: using reporters and long-read sequencing to identify copy number variation in experimental evolution. *J. Mol. Evol.* **91**, 356–368 (2023).
39. Lauer, S. et al. Single-cell copy number variant detection reveals the dynamics and diversity of adaptation. *PLoS Biol.* **16**, e3000069 (2018).
40. Loll-Krippleber, R. et al. A FACS-optimized screen identifies regulators of genome stability in *Candida albicans*. *Eukaryot. Cell* **14**, 311–322 (2015).
41. Marton, T. B. *Loss of Heterozygosity: Its Impact on Generating and Shaping Genetic Variations in Human Fungal Pathogen Candida albicans*. PhD thesis, Univ. Paris Cité (2020).
42. Marton, T., d'Enfert, C. & Legrand, M. Multiple stochastic parameters influence genome dynamics in a heterozygous diploid eukaryotic model. *J. Fungi* **8**, 650 (2022).
43. Feri, A. et al. Analysis of repair mechanisms following an induced double-strand break uncovers recessive deleterious alleles in the *Candida albicans* diploid genome. *mBio* https://doi.org/10.1128/mbio.01109-16 (2016).
44. Marton, T. et al. Identification of recessive lethal alleles in the diploid genome of a *Candida albicans* laboratory strain unveils a potential role of repetitive sequences in buffering their deleterious impact. *mSphere* **4**, e00709–e00718 (2019).
45. Jaitly, P. et al. A phylogenetically-restricted essential cell cycle progression factor in the human pathogen *Candida albicans*. *Nat. Commun.* **13**, 4256 (2022).
46. Marton, T. et al. Factors that influence bidirectional long-tract homozygosis due to double-strand break repair in *Candida albicans*. *Genetics* **218**, iyab028 (2021).
47. Lang, G. I. et al. Pervasive genetic hitchhiking and clonal interference in forty evolving yeast populations. *Nature* **500**, 571–574 (2013).
48. Veri, A. O. et al. Tuning Hsf1 levels drives distinct fungal morphogenetic programs with depletion impairing Hsp90 function and overexpression expanding the target space. *PLoS Genet.* **14**, e1007270 (2018).
49. Yang, F. et al. The fitness costs and benefits of trisomy of each *Candida albicans* chromosome. *Genetics* **218**, iyab056 (2021).
50. Kakade, P., Sircaik, S., Maufrais, C., Ene, I. V. & Bennett, R. J. Aneuploidy and gene dosage regulate filamentation and host colonization by *Candida albicans*. *Proc. Natl Acad. Sci. USA* **120**, e2218163120 (2023).
51. Vande Zande, P., Zhou, X. & Selmecki, A. The dynamic fungal genome: polyploidy, aneuploidy and copy number variation in response to stress. *Annu. Rev. Microbiol.* **77**, 341–361 (2023).
52. Lauer, S. & Gresham, D. An evolving view of copy number variants. *Curr. Genet.* **65**, 1287–1295 (2019).
53. Schoenfelder, K. P. & Fox, D. T. The expanding implications of polyploidy. *J. Cell Biol.* **209**, 485–491 (2015).
54. Fox, D. T., Soltis, D. E., Soltis, P. S., Ashman, T.-L. & Van de Peer, Y. Polyploidy: a biological force from cells to ecosystems. *Trends Cell Biol.* **30**, 688–694 (2020).
55. Kohanovski, I. et al. Aneuploidy can be an evolutionary diversion on the path to adaptation. *Mol. Biol. Evol.* **41**, msae052 (2024).
56. Hirakawa, M. P., Chyou, D. E., Huang, D., Slan, A. R. & Bennett, R. J. Parasex generates phenotypic diversity de novo and impacts drug resistance and virulence in *Candida albicans*. *Genetics* **207**, 1195–1211 (2017).
57. Feng, W. et al. Research of Mrr1, Cap1 and MDR1 in *Candida albicans* resistant to azole medications. *Exp. Ther. Med.* **15**, 1217–1224 (2018).
58. Li, W.-J. et al. FLO8 deletion leads to azole resistance by upregulating CDR1 and CDR2 in *Candida albicans*. *Res. Microbiol.* **170**, 272–279 (2019).
59. Narayanan, A. et al. Directed evolution detects supernumerary centric chromosomes conferring resistance to azoles in *Candida auris*. *mBio* **13**, e0305222 (2022).
60. Gómez-Raja, J., Andaluz, E., Magee, B., Calderone, R. & Larriba, G. A single SNP, G929T (Gly310Val), determines the presence of a functional and a non-functional allele of HIS4 in *Candida albicans* SC5314: detection of the non-functional allele in laboratory strains. *Fungal Genet. Biol.* **45**, 527–541 (2008).
61. Janbon, G., Sherman, F. & Rustchenko, E. Monosomy of a specific chromosome determines l-sorbose utilization: a novel regulatory mechanism in *Candida albicans*. *Proc. Natl Acad. Sci. USA* **95**, 5150–5155 (1998).
62. Glazier Virginia, E. et al. The *Candida albicans* reference strain SC5314 contains a rare, dominant allele of the transcription factor Rob1 that modulates filamentation, biofilm formation, and oral commensalism. *mBio* **14**, e01521–e01523 (2023).
63. White, T. C. The presence of an R467K amino acid substitution and loss of allelic variation correlate with an azole-resistant lanosterol 14alpha demethylase in *Candida albicans*. *Antimicrob. Agents Chemother.* **41**, 1488–1494 (1997).
64. Ene, I. V. et al. Global analysis of mutations driving microevolution of a heterozygous diploid fungal pathogen. *Proc. Natl Acad. Sci. USA* **115**, E8688–E8697 (2018).
65. Forche, A. et al. Selection of *Candida albicans* trisomy during oropharyngeal infection results in a commensal-like phenotype. *PLoS Genet.* **15**, e1008137 (2019).
66. Noble, S. M. & Johnson, A. D. Strains and strategies for large-scale gene deletion studies of the diploid human fungal pathogen *Candida albicans*. *Eukaryot. Cell* **4**, 298–309 (2005).
67. Shen, J., Guo, W. & Köhler, J. R. CaNAT1, a heterologous dominant selectable marker for transformation of *Candida albicans* and other pathogenic *Candida* species. *Infect. Immun.* **73**, 1239–1242 (2005).
68. Anderson, J. B. et al. Mode of selection and experimental evolution of antifungal drug resistance in *Saccharomyces cerevisiae*. *Genetics* **163**, 1287–1298 (2003).
69. Todd, R. T., Braverman, A. L. & Selmecki, A. Flow cytometry analysis of fungal ploidy. *Curr. Protoc. Microbiol.* **50**, e58 (2018).
70. Bushnell, B. BBTools Software Package http://sourceforge.net/projects/bbmap (Joint Genome Institute, 2014).
71. Skrzypek, M. S. et al. The *Candida* Genome Database (CGD): incorporation of Assembly 22, systematic identifiers and visualization of high throughput sequencing data. *Nucleic Acids Res.* **45**, D592–D596 (2017).
72. Li, H. Aligning sequence reads, clone sequences and assembly contigs with BWA-MEM. Preprint at https://arxiv.org/abs/1303.3997 (2013).
73. Danecek, P. et al. Twelve years of SAMtools and BCFtools. *Gigascience* **10**, giab008 (2021).
74. Andrews, S. FastQC: A Quality Control Tool for High Throughput Sequence Data [Online]. http://www.bioinformatics.babraham.ac.uk/projects/fastqc/ (2010).
75. Okonechnikov, K., Conesa, A. & García-Alcalde, F. Qualimap 2: advanced multi-sample quality control for high-throughput sequencing data. *Bioinformatics* **32**, 292–294 (2016).

76. Ewels, P., Magnusson, M., Lundin, S. & Käller, M. MultiQC: summarize analysis results for multiple tools and samples in a single report. *Bioinformatics* **32**, 3047–3048 (2016).
77. Abbey, D. A. et al. YMAP: a pipeline for visualization of copy number variation and loss of heterozygosity in eukaryotic pathogens. *Genome Med.* **6**, 100 (2014).
78. Thorvaldsdóttir, H., Robinson, J. T. & Mesirov, J. P. Integrative Genomics Viewer (IGV): high-performance genomics data visualization and exploration. *Brief. Bioinform.* **14**, 178–192 (2013).
79. Van der Auwera, G. A. & O'Connor, B. D. *Genomics in the Cloud: Using Docker, GATK, and WDL in Terra* (O'Reilly Media, 2020).
80. Cingolani, P. et al. A program for annotating and predicting the effects of single nucleotide polymorphisms, SnpEff: SNPs in the genome of *Drosophila melanogaster* strain w1118; iso-2; iso-3. *Fly* **6**, 80–92 (2012).
81. Robinson, J. T., Thorvaldsdóttir, H., Wenger, A. M., Zehir, A. & Mesirov, J. P. Variant review with the Integrative Genomics Viewer. *Cancer Res.* **77**, e31–e34 (2017).
82. Zhou, X. et al. Data supporting 'Single-cell detection of copy number changes reveals dynamic mechanisms of adaptation to antifungals in *Candida albicans*'. *University Digital Conservancy* https://conservancy.umn.edu/items/1e092a2a-f661-483f-91a7-3ff9eba64602 (2024).
83. Zhou, X., Scott, N. & Selmecki A. Code supporting 'Single-cell detection of copy number changes reveals dynamic mechanisms of adaptation to antifungals in *Candida albicans*'. *GitHub*. https://github.com/selmeckilab/2024_BFPGFP_NMICROBIOL (2024).

Acknowledgements

We thank R. T. Todd, P. V. Zande and U. Oggenfuss for helpful discussion and feedback on the manuscript; M. Legrand for the BFP/GFP plasmids pECC596 and pECC727; L. E. Cowen for the tetO plasmid pLC605; and the University of Minnesota Flow Cytometry Resource (UFCR) for technical support. Funding for this work was provided by the National Institutes of Health (R01 AI143689), the National Science Foundation (NSF DBI-232051) and the Burroughs Wellcome Fund Investigator in the Pathogenesis of Infectious Diseases Award (#1020388) to A.S., and the Swanson–Holcomb Undergraduate Research Fund at Gustavus Adolphus College to C.L.B. and L.S.B.

Author contributions

X.Z. and A.S. conceptualized and designed the study. The experimental work was performed by X.Z., A.H., N.V.S., A.B. and C.L.B. Data analysis was performed by X.Z, N. Scott, N. Soisangwan and L.B. X.Z and A.S. wrote the original draft and together with L.S.B. edited and reviewed the manuscript. A.S. acquired the primary funding for this work. L.S.B. and S.G.F provided additional experimental resources.

Competing interests

The authors declare no competing interests.

Additional information

Extended data is available for this paper at https://doi.org/10.1038/s41564-024-01795-7.

Supplementary information The online version contains supplementary material available at https://doi.org/10.1038/s41564-024-01795-7.

Correspondence and requests for materials should be addressed to Anna Selmecki.

Peer review information *Nature Microbiology* thanks David Gresham and the other, anonymous, reviewer(s) for their contribution to the peer review of this work. Peer reviewer reports are available.

https://doi.org/10.1038/s41564-024-01795-7

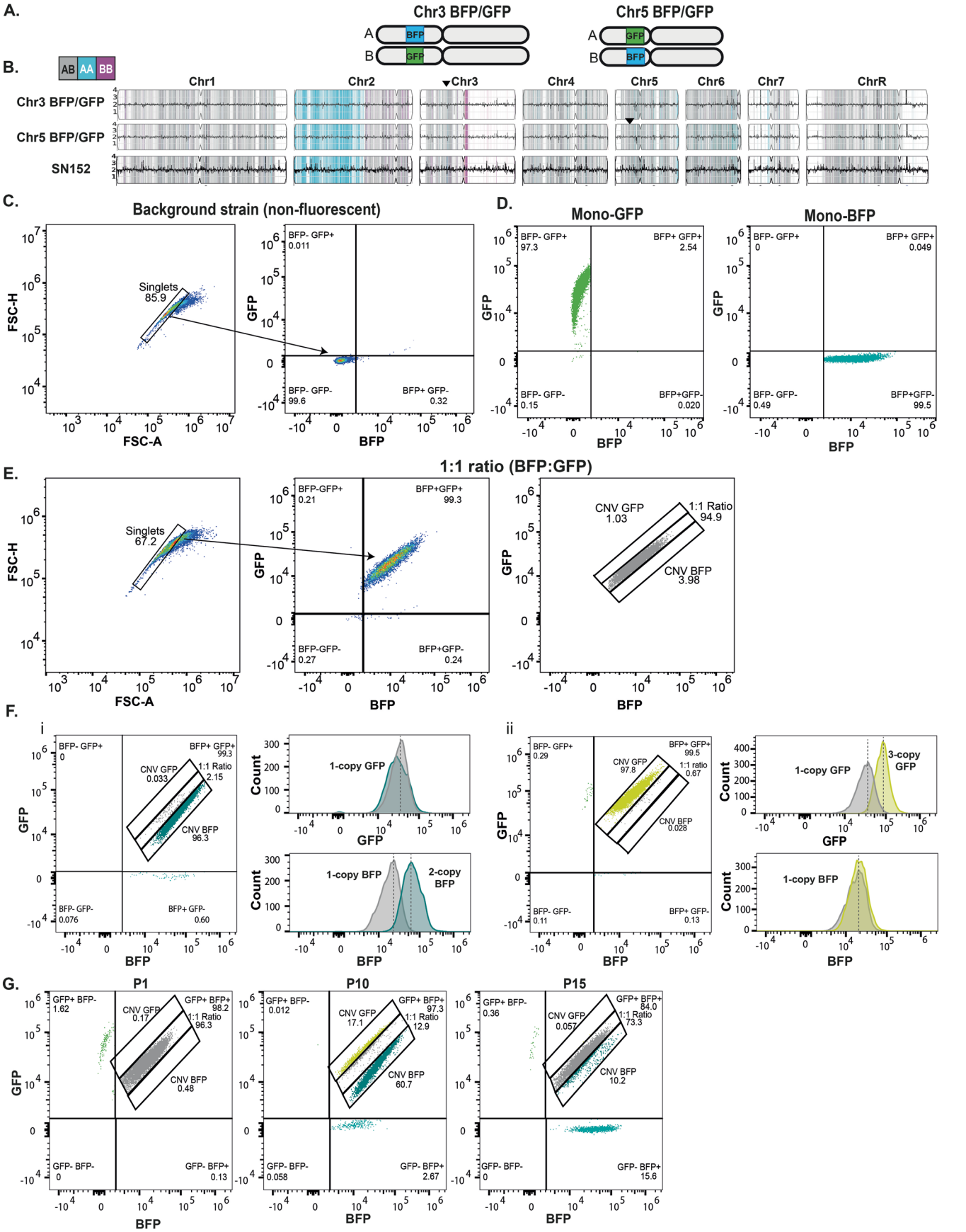

Extended Data Fig. 1 | See next page for caption.

https://doi.org/10.1038/s41564-024-01795-7

Extended Data Fig. 1 | Detection of both CNV and LOH using a BFP/GFP flow cytometry system. A. Schematic of the BFP and GFP reporter strains. BFP and GFP are tagged on the left arms of Chr3 and Chr5. **B**. Whole-genome sequencing (WGS) data from the Chr3 BFP/GFP, Chr5 BFP/GFP reporter strains, and the background strain Sn152. WGS data are plotted as the log2 ratio and converted to chromosome copy number (y-axis, 1-4 copies) as a function of chromosome position (x-axis, Chr1-ChrR)[8]. The baseline ploidy was determined by propidium iodide (PI)-DNA staining (Table S1). Haplotypes relative to the reference genome SC5314 are indicated: grey is heterozygous AB, magenta is homozygous B, and cyan is homozygous A. Arrowheads indicate the position of the BFP/GFP loci. **C-E** Representative scatter plots for the control strains, with fluorescence intensity of BFP plotted on the x-axis and GFP on the y-axis. The four quadrants include non-fluorescent cells (BFP- GFP-), BFP only cells (BFP + GFP-), GFP only cells (BFP- GFP +) and dual-fluorescent cells (BFP + GFP +). Gating strategy for detection of singlets for non-fluorescent cells (**C**) and mono-fluorescent control strains, mono-GFP (D, left) and mono-BFP (D, right). **E**. Dual-fluorescent progenitor strains after gating for singlets with a rectangular gate drawn around the cells indicating a 1:1 ratio of BFP:GFP. Extensions of this gate represent changes in the 1:1 ratio due to copy number amplification of BFP or GFP (CNV BFP and CNV GFP). **F**. Representative scatter plots for CNV cells with histograms indicating the fluorescence intensity of BFP or GFP compared to the 1:1 ratio control. Copy numbers were determined by the median fluorescence intensity. i: CNV GFP, ii: CNV BFP. **F**. Flow cytometry detection of single cells within a population that acquired CNV and LOH of BFP and/or GFP during *in vitro* evolution. One representative example of a FLC-evolved lineage (Chr3_FLC4_L9) with BFP and GFP fluorescence changes at passages P1, P10, and P15 with population fractions indicated. **C-G:** Colors indicate 1:1 ratio of BFP:GFP (gray), CNV BFP (dark cyan), CNV GFP (yellow), GFP only (green), and BFP only (sky blue).

https://doi.org/10.1038/s41564-024-01795-7

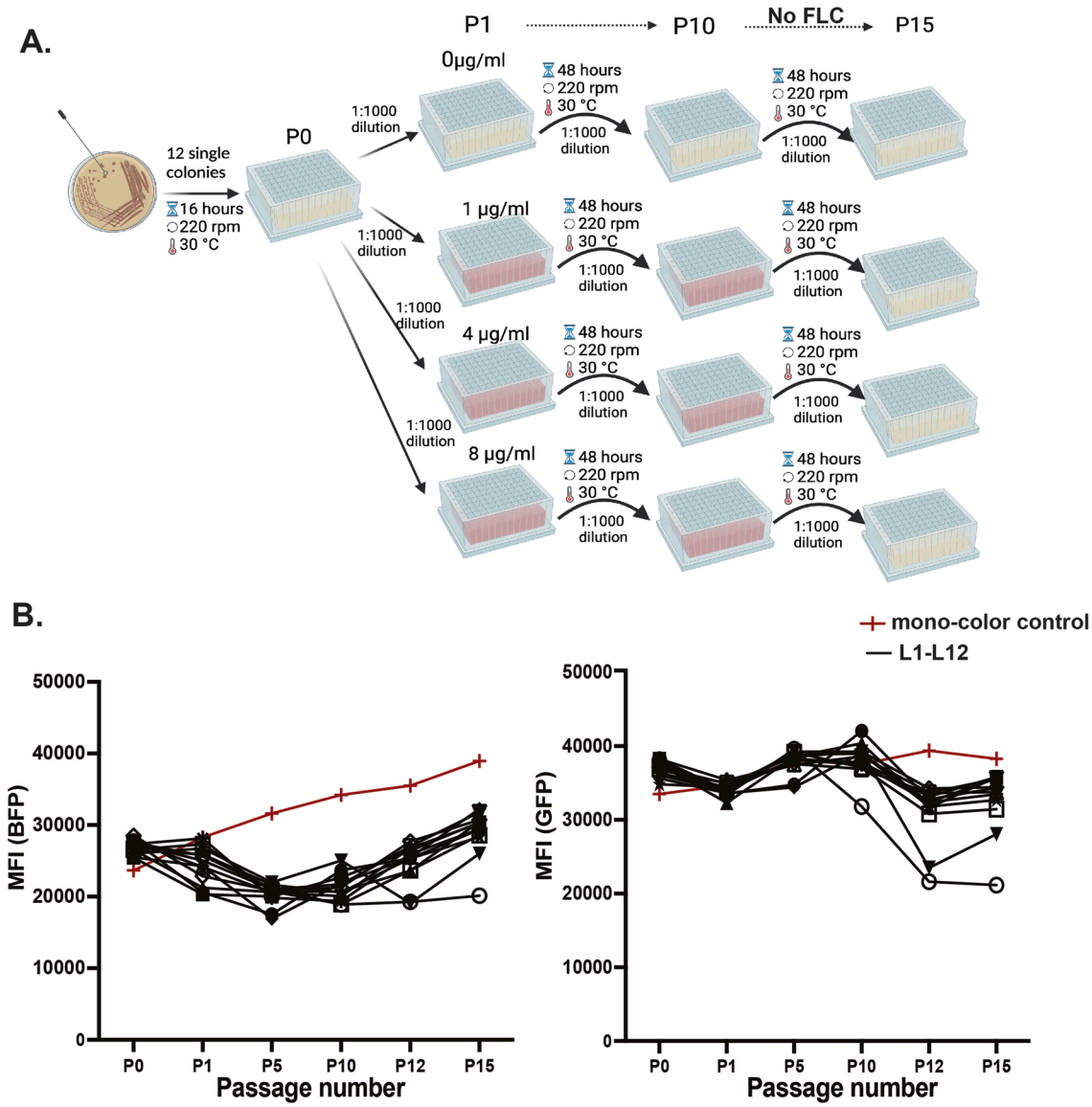

Extended Data Fig. 2 | Schematic of the BFP/GFP *in-vitro* evolution experiment and flow cytometry controls. A. Twelve single colonies from each BFP/GFP strain were inoculated into independent wells and cultured for 16 hrs. These twelve P0 lineages were diluted and split into four treatment conditions either in the absence or presence of FLC (0 µg/ml, 1 µg/ml, 4 µg/ml, and 8 µg/ml). The lineages were passaged every 48 hrs at 1:1000 dilution. After 10 passages, no FLC was added, and all lineages were cultured only in rich media (0 µg/ml, YPAD) for another 5 passages with the same serial dilutions. Cells from every passage were collected and stored at −80 °C. Figure created in BioRender.com. **B**. Median fluorescence intensity (MFI) of BFP (left) and GFP (right) of the no drug (0 µg/ml FLC) controls (black, twelve lineages L1-L12) and the mono-fluorescent control strains (red) at passages 0, 1, 5, 10, 12, and 15. Controls for day-to-day fluctuations in fluorescent intensity caused by variations in growth status and flow cytometer readings.

https://doi.org/10.1038/s41564-024-01795-7

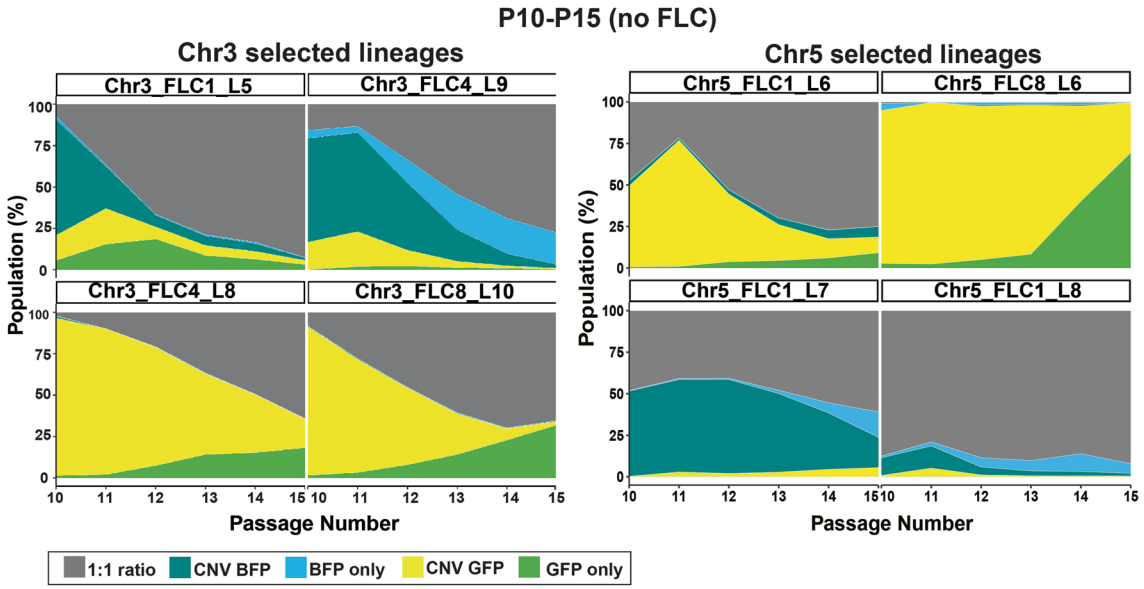

Extended Data Fig. 3 | Population dynamics after FLC removal (passages 10-15). Flow cytometry data plotted for populations where the rate of decrease (S_{down}) and rate of increase (S_{up}) was calculated (Table S3). Stacked population fractions after removal of the drug (P10-P15) for select Chr3 lineages (left) and Chr5 lineages (right).

https://doi.org/10.1038/s41564-024-01795-7

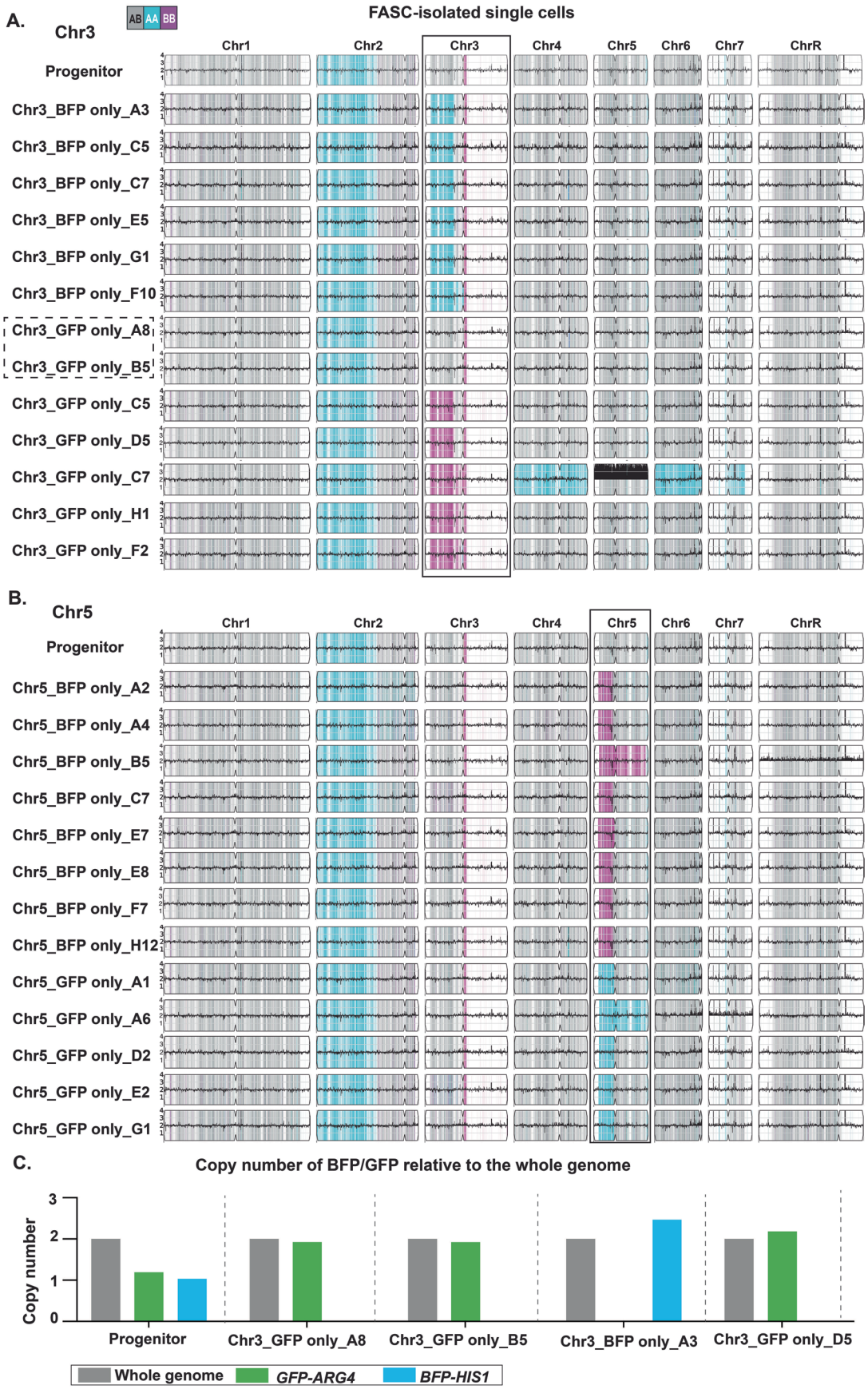

Extended Data Fig. 4 | See next page for caption.

https://doi.org/10.1038/s41564-024-01795-7

Extended Data Fig. 4 | FACS-isolated single cells exhibited loss of heterozygosity on tagged chromosomes. Genotypes of single cells obtained from the progenitor strains via fluorescence activated cell sorting (FACS) after overnight growth in the absence of drug. **A.** Chr3 BFP/GFP and (**B**) Chr5 BFP/GFP progenitor strains. Whole genome sequencing (WGS) data plotted Extended Data Fig. 1B. The baseline chromosome copy number (ploidy) was determined by flow cytometry (Table S1). Haplotypes indicated by the color: gray is heterozygous AB, magenta is homozygous B, cyan is homozygous A. Dashed box highlights two strains that underwent gene conversion events involving LOH only at GFP tagged regions. Boxes indicated the tagged chromosome. **C.** Gene conversion of the BFP/GFP locus detected in two FACS-isolated single cells. Copy numbers of *GFP-ARG4* or *BFP-HIS1* were determined by average read depth at the *GFP-ARG4* or *BFP-HIS1* loci relative to average whole-genome read depth for: i) the Chr3 BFP/GFP progenitor; ii) two independent FACS sorted single cells from Extended Data Fig. 4A that were GFP only but heterozygous for the rest of Chr3 (dashed box); and iii) two FACS sorted single cells from Extended Data Fig. 4A that were BFP only or GFP only and acquired large LOH regions of Chr3. The progenitor and single cells in this copy number analysis were all euploid.

https://doi.org/10.1038/s41564-024-01795-7

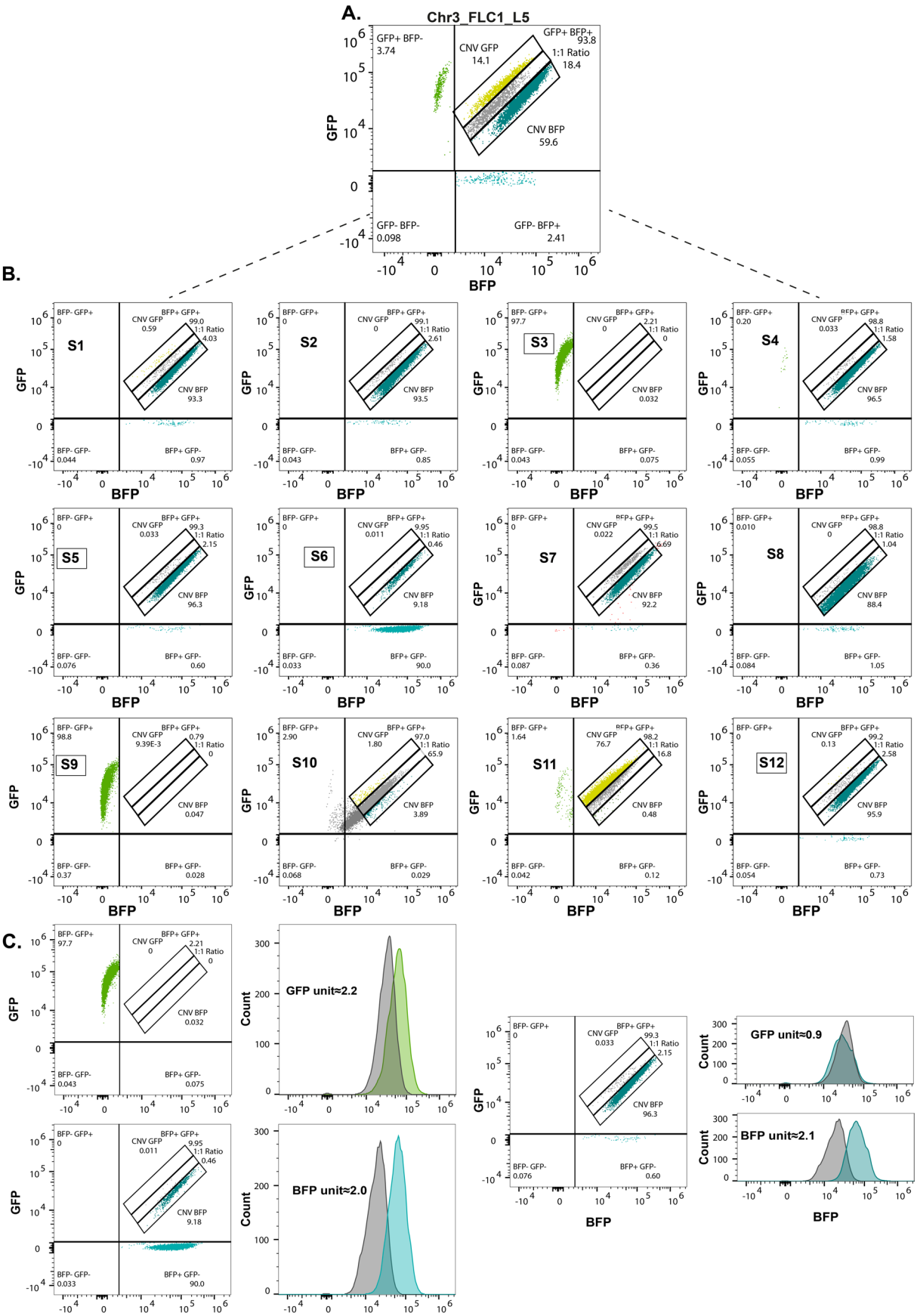

Extended Data Fig. 5 | Fluorescence analysis of single colonies and estimation of DNA copy number. A. Scatter plot for Chr3_FLC1_L5 total population at BFP (x-axis) vs GFP (y-axis). **B**. Scatter plots of 12 single colonies (S1-S12) randomly selected from Chr3_FLC1_L5. Single colonies S3, S5, S6, S9, and S12 selected for WGS are indicated with a box around their name. **C**. Calculation of fluorescent units: median fluorescence intensity of analyzed cells were normalized by the median fluorescence intensity of one copy BFP or GFP controls.

https://doi.org/10.1038/s41564-024-01795-7

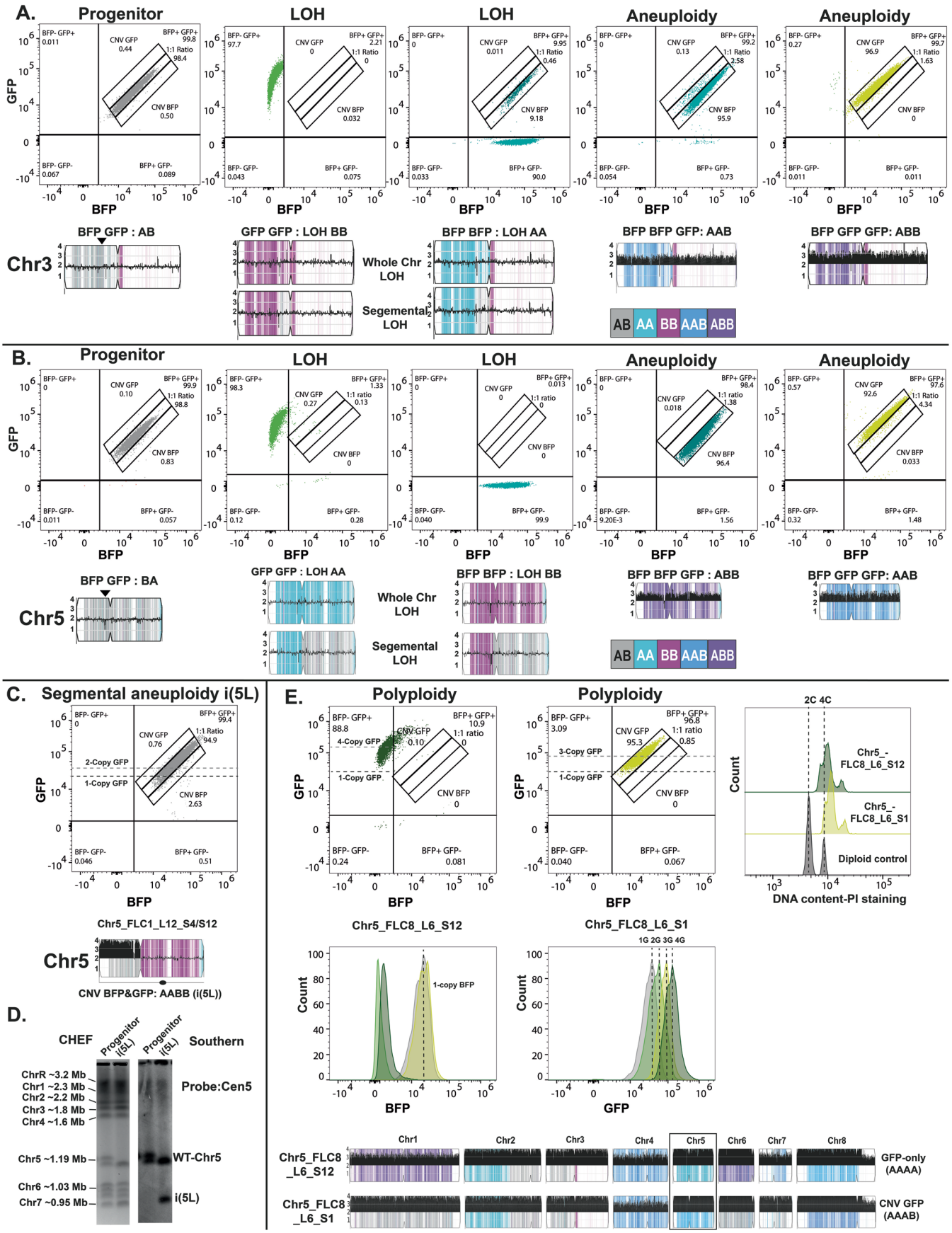

Extended Data Fig. 6 | See next page for caption.

https://doi.org/10.1038/s41564-024-01795-7

Extended Data Fig. 6 | Fluorescent phenotype detects genotype changes including LOH, aneuploidy, and polyploidy. Representative flow cytometry scatter plots for four different fluorescent phenotypes: GFP-only, BFP-only, CNV BFP, and CNV GFP and the corresponding genotypes of the tagged chromosomes as detected by WGS. Both whole chromosome and segmental chromosome events are indicated. Inverted triangles indicate the BFP/GFP tagged locus. WGS data plotted as in Extended Data Fig. 1B. The baseline chromosome copy number (ploidy) was determined by flow cytometry (Table S1). Haplotypes are indicated by the color: gray is heterozygous AB, magenta is homozygous B, cyan is homozygous A, purple is ABB, and blue is AAB. **A**. Chr3 BFP/GFP progenitor strain (euploid heterozygous) and representative evolved colonies with Chr3 GFP-only (LOH BB), Chr3 BFP-only (LOH AA), Chr3 CNV GFP (aneuploid ABB), Chr3 CNV BFP (aneuploid AAB). **B**. Chr5 BFP/GFP progenitor strain (euploid heterozygous) and representative evolved colonies with Chr5 GFP-only (LOH AA) Chr5 BFP-only (LOH BB), Chr5 CNV GFP (aneuploid AAB), and Chr5 CNV BFP (aneuploid ABB). **C&D**. Segmental amplification of Chr5L in an isochromosome structure. Flow cytometry plot indicating a doubling of both the Chr5 BFP & GFP fluorescence units and the corresponding genotype for FLC evolved lineages (Chr5_FLC1_L12_S4/12). **D**. CHEF karyotype gel stained with ethidium bromide (left) of the progenitor strain and an i(5L) strain from Extended Data Fig. 6C and Southern blot (right) probed with the centromere of Chr5 (*CEN5*). **E**. Polyploid cells detected by combined fluorescent units ~4. Scatter plots (Left) for two single colonies indicating BFP and GFP fluorescence with histograms indicating the copies of BFP or GFP compared to 1:1 ratio control. PI-DNA staining of these two colonies with a diploid control (Right). Bottom: WGS data for two tetraploid cells. Black dashed lines in flow cytometry scatter plots indicate the median fluorescence intensity of 1-copy GFP (1 G, 1:1 ratio control), 2-copy GFP (2 G, Chr5 LOH AA from B), 3-copy GFP (3 G, Chr5_FLC8_L6_S1), and 4-copy GFP (4 G, Chr5_FLC8_L6_S12). Gates in all scatter plots were generated with controls as described in Fig. 1.

https://doi.org/10.1038/s41564-024-01795-7

Extended Data Fig. 7 | See next page for caption.

https://doi.org/10.1038/s41564-024-01795-7

Extended Data Fig. 7 | Detection of copy number and allele ratio changes by whole genome sequencing for representative single colonies. WGS data plotted as the log2 ratio and converted to chromosome copy number (y-axis, 1-4 copies) as a function of chromosome position (x-axis, Chr1-ChrR) using YMAP[8]. The baseline chromosome copy number (ploidy) was determined by flow cytometry (Table S1). Haplotypes indicated by the color: gray designate heterozygous AB, magenta for homozygous B, cyan for homozygous A, purple for ABB, and blue for AAB. **A**. WGS data for Chr3-tagged BFP/GFP single colonies. **B**. WGS data for Chr5-tagged BFP/GFP single colonies with representative aneuploidies. **C**. WGS data for Chr5-tagged single colonies that were CNV BFP by phenotype but had no detectable Chr5 CNV after sequencing. All single colonies were isolated from in vitro FLC-evolved lineages at P10 (Extended Data Fig. 5 and Methods).

https://doi.org/10.1038/s41564-024-01795-7

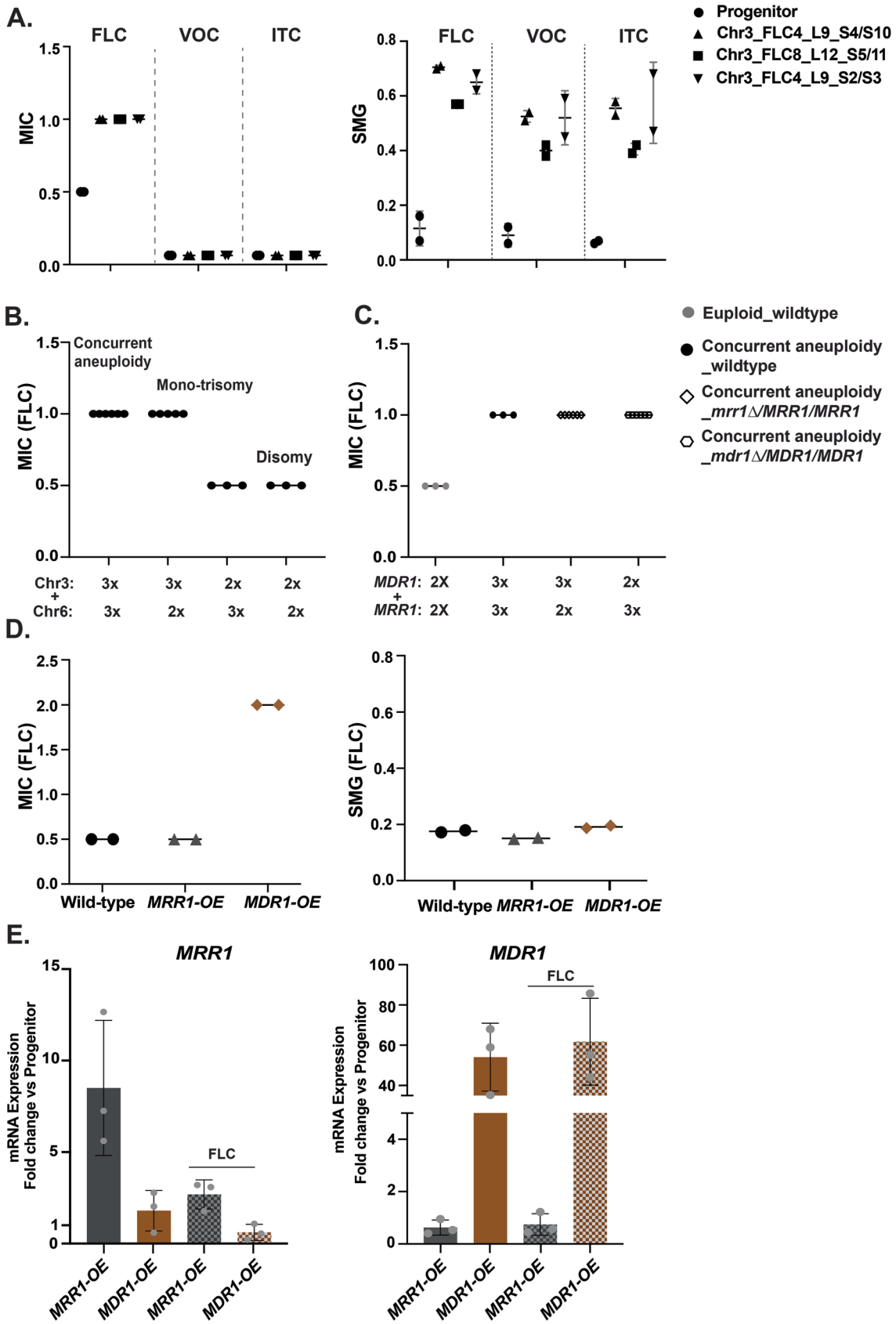

Extended Data Fig. 8 | See next page for caption.

https://doi.org/10.1038/s41564-024-01795-7

Extended Data Fig. 8 | Chr3 trisomy alone confers 2-fold increased MIC in FLC. A. 24 hr MIC and 48 hr SMG for single colonies with Chr3 and Chr6 trisomy in fluconazole (FLC), voriconazole (VOC) and itraconazole (ITC) with the progenitor as the control. **B**. MIC of single colonies with Chr3 and Chr6 aneuploidy (concurrent aneuploidy) (n = 6 strains), Chr3 trisomy or Chr6 trisomy (mono-trisomy) (n = 4 and 3 strains), and euploidy (disomy) (n = 3 strains) in FLC. **A**&**B**. Each dot represents the average of three technical replicates for each strain. **C**. MIC of *MRR1* or *MDR1* heterozygous deletion mutants (n = 5 strains) in concurrent trisomy aneuploidy background with euploid wildtype and concurrent aneuploidy as the control in FLC. **D**. Overexpression (OE) of *MDR1* or *MRR1* leads to an increase in MIC but no change in drug tolerance quantified as the supra-MIC growth (SMG) at 48 hr. MIC (left) and SMG (right) of *MDR1*- and *MRR1*-OE strains with the wild-type control. **C**&**D**. Each dot represents the average of three technical replicates for a single transformant. **A**-**D**. The line and error bars indicate the median and standard deviation across all strains with the same genotype. **E**. mRNA expression fold change of *MRR1* (left) and *MDR1*(right) in *MRR1*-OE and *MDR1-OE* strains relative to the progenitor with *TEF1* on Chr2 as the control. Expression changes were tested in YPAD and YPAD + 1 μg/ml FLC conditions. Values are mean ± SEM calculated from three biological replicates. Error bars indicate the standard deviation across three biological replicates.

https://doi.org/10.1038/s41564-024-01795-7

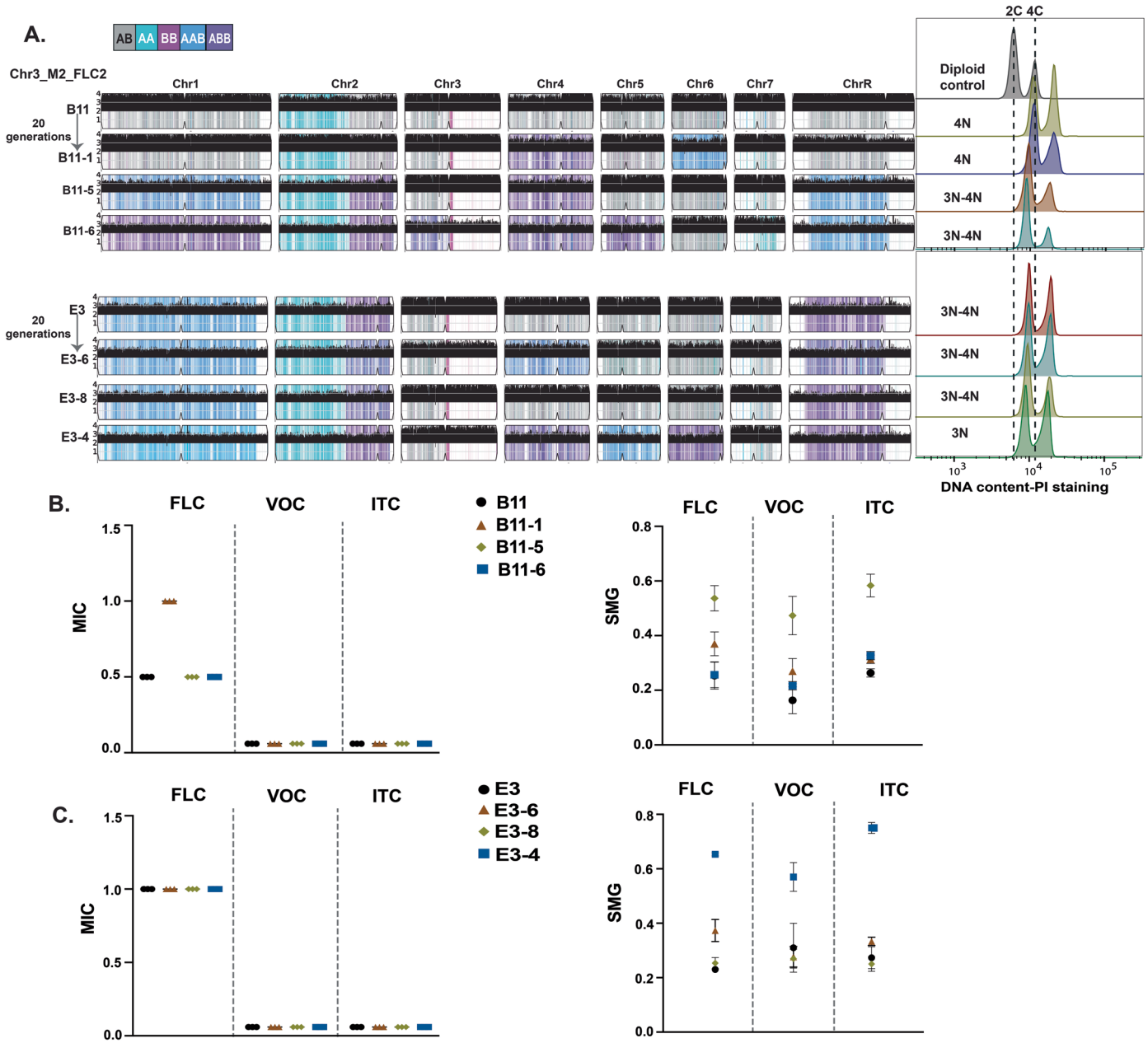

Extended Data Fig. 9 | Genomic instability of polyploid cells and its fitness consequence. A. Passaging of polyploid colonies *in vitro* results in chromosome loss. WGS data of two polyploid colonies from the same mouse, Chr3_M2_FLC2_B11 and Chr3_M2_FLC2_E3, with 3 evolved single colonies. Ploidy level indicated to the right using propidium iodide staining of DNA content. WGS data plotted as in Extended Data Fig. 1B. **B&C.** MIC and SMG values for the two mouse-derived polyploid colonies: B11(B) and E3 (C) and their evolved progeny. Each dot represents the average of three technical replicates and error bars indicate the standard deviations across three technical replicates.

nature portfolio

Corresponding author(s): Anna Selmecki

Last updated by author(s): Jul 18, 2024

Reporting Summary

Nature Portfolio wishes to improve the reproducibility of the work that we publish. This form provides structure for consistency and transparency in reporting. For further information on Nature Portfolio policies, see our Editorial Policies and the Editorial Policy Checklist.

Statistics

For all statistical analyses, confirm that the following items are present in the figure legend, table legend, main text, or Methods section.

n/a	Confirmed	
☐	☒	The exact sample size (*n*) for each experimental group/condition, given as a discrete number and unit of measurement
☐	☒	A statement on whether measurements were taken from distinct samples or whether the same sample was measured repeatedly
☐	☒	The statistical test(s) used AND whether they are one- or two-sided *Only common tests should be described solely by name; describe more complex techniques in the Methods section.*
☐	☒	A description of all covariates tested
☐	☒	A description of any assumptions or corrections, such as tests of normality and adjustment for multiple comparisons
☐	☒	A full description of the statistical parameters including central tendency (e.g. means) or other basic estimates (e.g. regression coefficient) AND variation (e.g. standard deviation) or associated estimates of uncertainty (e.g. confidence intervals)
☐	☒	For null hypothesis testing, the test statistic (e.g. *F*, *t*, *r*) with confidence intervals, effect sizes, degrees of freedom and *P* value noted *Give P values as exact values whenever suitable.*
☒	☐	For Bayesian analysis, information on the choice of priors and Markov chain Monte Carlo settings
☒	☐	For hierarchical and complex designs, identification of the appropriate level for tests and full reporting of outcomes
☒	☐	Estimates of effect sizes (e.g. Cohen's *d*, Pearson's *r*), indicating how they were calculated

Our web collection on statistics for biologists contains articles on many of the points above.

Software and code

Policy information about availability of computer code

Data collection	Flow cytometry raw data collection was performed on a Cytek Aurora flow cytometer (R0021) running SpectroFlo (V3.1.2). Florescence activated cell sorting was performed on a BD FACSAria II analyzer (P07800142) running BD FACSDiva software. Optical density of yeast cells was performed on a BioTek Epoch2 Plate reader running Gen5. RT-PCR was performed on a Bio-Rad CFX machine running Maestro software (V2.0).
Data analysis	The R programming language (v4.1.2), GATK (v4.1.2), bcftools (v1.17), IGV(v2.8.2), YMAP(v1.0), BBDuk (BBTools v38.94), BWA-MEM (v0.7.17), SnpEff (v5.0e), Samtools (v1.10), FastQC (v0.11.7), Qualimap (v2.2.2-dev), MultiQC (v1.16), FlowJo (v10.8.1), bcl-convert (v3.9.3),GraphPad Prism(v10.11). All computational scripts used for stacked plots and whole genome sequence alignment and variant calling will be publicly available through the Selmecki Lab Github page (https://github.com/selmeckilab).

For manuscripts utilizing custom algorithms or software that are central to the research but not yet described in published literature, software must be made available to editors and reviewers. We strongly encourage code deposition in a community repository (e.g. GitHub). See the Nature Portfolio guidelines for submitting code & software for further information.

Data

Policy information about availability of data

All manuscripts must include a data availability statement. This statement should provide the following information, where applicable:

- Accession codes, unique identifiers, or web links for publicly available datasets
- A description of any restrictions on data availability
- For clinical datasets or third party data, please ensure that the statement adheres to our policy

All whole genome sequences (raw FASTQ files) are available in the Sequence Read Archive repository under BioProject PRJNA973218. All BioSample numbers are listed in Table S1. All the flow cytometry raw data (.fcs files) are available at the Data Repository for University of Minnesota (https://doi.org/10.13020/pg0z-ag23). All the strains used in this study are available upon request.

Research involving human participants, their data, or biological material

Policy information about studies with human participants or human data. See also policy information about sex, gender (identity/presentation), and sexual orientation and race, ethnicity and racism.

Reporting on sex and gender	N/A
Reporting on race, ethnicity, or other socially relevant groupings	N/A
Population characteristics	N/A
Recruitment	N/A
Ethics oversight	N/A

Note that full information on the approval of the study protocol must also be provided in the manuscript.

Field-specific reporting

Please select the one below that is the best fit for your research. If you are not sure, read the appropriate sections before making your selection.

☒ Life sciences ☐ Behavioural & social sciences ☐ Ecological, evolutionary & environmental sciences

For a reference copy of the document with all sections, see nature.com/documents/nr-reporting-summary-flat.pdf

Life sciences study design

All studies must disclose on these points even when the disclosure is negative.

Sample size	For the in vitro experiments, 12 replicate lineages were randomly initiated from each progenitor strain. 12 replicate lineages were sufficient to represent the diversity of copy number changes that occur in these populations, including gain and loss of each haplotype represented by the BFP or GFP locus. Twelve replicate lineages were also ideal for the 96-well plate layout, enabling us to perform high-throughput flow cytometry sampling. All 12 replicate lineages were evolved for 10 passages under 4 different fluconazole (FLC) concentrations: (i) YPAD with 0 µg/ml FLC, (ii) YPAD with 1 µg/ml FLC, (iii) YPAD with 4 µg/ml FLC, and (iv) YPAD with 8 µg/µml FLC. All 96 lineages were evolved, archived, and analyzed. For the in vivo experiments, a total of 40 mice were used for this study. 20 mice were used for each yeast progenitor strain. 5 mice were used for each of the 4 different treatments: PBS only, 0.5, 2, or 5 mg/kg FLC. Up to 96 fungal single colonies were recovered from the kidney of each mouse and all recovered single colonies were processed and analyzed. Based on our previous data, the standard deviation in kidney fungal burden (log10 CFU/g tissue) had a normal distribution with a standard deviation of 0.5. Therefore having 5 mice per group gives 80% power to detect a 1-log reduction in oral fungal burden relative to the control mice with an alpha of 0.05. For FACS, each single cell were sorted into a single well of 96-well plate therefore 96 GFP-only or BFP-only single cells were sorted each progenitor and total 384 sorted single cells were processed and analyzed.
Data exclusions	No data were excluded from this study.
Replication	All experimental assays including MIC, SMG, growth curve, RT-qPCR, head-to-head competitive assays, and flow cytometry for determining LOH rates were replicated at least three independent times. All replications were used in our analyses and gave similar results. Additional biological replicates are described above in 'sample size'.
Randomization	BFP and GFP were randomly integrated into A or B homologue when designing the progenitor strains. The 12 in vitro lineages were initiated

Randomization	from 12 colonies randomly picked from each progenitor strain. The mice were randomly selected for infection with the various strains and for treatment with the different doses of fluconazole. Single colonies were randomly recovered from CFU plates.
Blinding	The investigators were blinded to the identities of the infecting strains during all mouse and cell-sorting experiments.

Reporting for specific materials, systems and methods

We require information from authors about some types of materials, experimental systems and methods used in many studies. Here, indicate whether each material, system or method listed is relevant to your study. If you are not sure if a list item applies to your research, read the appropriate section before selecting a response.

Materials & experimental systems

n/a	Involved in the study
☒	☐ Antibodies
☒	☐ Eukaryotic cell lines
☒	☐ Palaeontology and archaeology
☐	☒ Animals and other organisms
☒	☐ Clinical data
☒	☐ Dual use research of concern
☒	☐ Plants

Methods

n/a	Involved in the study
☒	☐ ChIP-seq
☐	☒ Flow cytometry
☒	☐ MRI-based neuroimaging

Animals and other research organisms

Policy information about studies involving animals; ARRIVE guidelines recommended for reporting animal research, and Sex and Gender in Research

Laboratory animals	The animal experiments were performed using 6-week-old, male, outbred CD-1 mice. The mice were randomly selected for infection with the various strains and for treatment with the different doses of fluconazole. The investigators were blinded to the identities of the infecting strains.
Wild animals	The study did not involve wild animals.
Reporting on sex	Only male outbred CD-1 mice were included in this study.
Field-collected samples	The study did not involve samples collected from the field.
Ethics oversight	All animal work was approved by the Institutional Animal Care and Use Committee (IACUC) of the Lundquist Institute for Biomedical Innovation at Harbor-UCLA Medical Center under the animal welfare assurance number D16-00213. The mice were housed at 20°C on a 12 hrs light/dark cycle in ambient humidity.

Note that full information on the approval of the study protocol must also be provided in the manuscript.

Plants

Seed stocks	N/A
Novel plant genotypes	N/A
Authentication	N/A

Flow Cytometry

Plots

Confirm that:

☒ The axis labels state the marker and fluorochrome used (e.g. CD4-FITC).

☒ The axis scales are clearly visible. Include numbers along axes only for bottom left plot of group (a 'group' is an analysis of identical markers).

☒ All plots are contour plots with outliers or pseudocolor plots.

☒ A numerical value for number of cells or percentage (with statistics) is provided.

Methodology

Sample preparation	For fluorescent change detection: all isolates including controls were inoculated in 2% dextrose YPAD from frozen stocks and incubated for 12-16 hrs at 30C, 220 rpm. Cultures were diluted in PBS. For FACS: BFP/GFP tagged progenitors were plated on YPAD agar from frozen stocks and incubated for 24 hrs at 30C. At least three single colonies of each strain were selected and inoculated into 50 ml of 2% dextrose YPAD and grown for 36 hrs at 30C, 220rpm. These cultures were diluted in PBS+5mM EDTA then passed through cell strainer (70µm) for FACS. For ploidy: Isolates were inoculated in 2% dextrose YPAD from frozen stocks and incubated overnight at 30C, 220 rpm to a cell density of 1x107 cells/ml. Cultures were gently spun down at 3000 rpm for 3 minutes and the supernatant was removed. Cell pellets were resuspended in 70% ethanol, then washed twice with 50 mM sodium citrate. Following washing, cells were spun down and resuspended in 50 mM sodium citrate containing 0.5 mg/ml RNase A. Cells were treated with RNase A at 37C for at least two hrs, then stained with 25 µg/ml propidium iodide (PI) at 37C in the dark overnight. Samples were diluted in 50 mM sodium citrate.
Instrument	Cytek Aurora flow cytometer (R0021) and BD FACSAria II analyzer (P07800142)
Software	Flow data was collected using SpectroFlo (V3.1.2) and FACSDiva (V8.0.1); Flow data were analysed using FlowJo (v10.8.1).
Cell population abundance	At least 10000 cells were processed for all flow experiments except FSCS. At least 100000 cells were processed for single cell sorting to get sufficient single cells with LOH.
Gating strategy	For fluorescent changes and FACS: Non-fluorescent, mono-fluorescent, and dual-fluorescent controls were used. We removed doublets (FSC-A vs FSC-H) and drew gates to fit the non-fluorescent/dead cells (BFP- GFP-), mono-fluorescent BFP (BFP+ GFP-), mono-fluorescent GFP (BFP- GFP+), and the dual-fluorescent cells (BFP+ GFP+). Within the dual-fluorescent gate, BFP/GFP progenitor strains with only one copy of both BFP and GFP were used to generate a 1:1 ratio (BFP vs GFP) gate. Dual-fluorescent cells that were outside this 1:1 gate were further gated as CNVs, due to increased fluorescence of BFP, GFP, or both BFP&GFP. For ploidy analysis: After removing doublets, non-stained cells were used as negative control. The diploid progenitor control was used to define G1 (1C) and G2 (2C) peaks.

☒ Tick this box to confirm that a figure exemplifying the gating strategy is provided in the Supplementary Information.